INFORMATION TO USERS

This material was produced from a microfilm copy of the original document. While the most advanced technological means to photograph and reproduce this document have been used, the quality is heavily dependent upon the quality of the original submitted.

The following explanation of techniques is provided to help you understand markings or patterns which may appear on this reproduction.

1. The sign or "target" for pages apparently lacking from the document photographed is "Missing Page(s)". If it was possible to obtain the missing page(s) or section, they are spliced into the film along with adjacent pages. This may have necessitated cutting thru an image and duplicating adjacent pages to insure you complete continuity.

2. When an image on the film is obliterated with a large round black mark, it is an indication that the photographer suspected that the copy may have moved during exposure and thus cause a blurred image. You will find a good image of the page in the adjacent frame.

3. When a map, drawing or chart, etc., was part of the material being photographed the photographer followed a definite method in "sectioning" the material. It is customary to begin photoing at the upper left hand corner of a large sheet and to continue photoing from left to right in equal sections with a small overlap. If necessary, sectioning is continued again — beginning below the first row and continuing on until complete.

4. The majority of users indicate that the textual content is of greatest value, however, a somewhat higher quality reproduction could be made from "photographs" if essential to the understanding of the dissertation. Silver prints of "photographs" may be ordered at additional charge by writing the Order Department, giving the catalog number, title, author and specific pages you wish reproduced.

5. PLEASE NOTE: Some pages may have indistinct print. Filmed as received.

Xerox University Microfilms
300 North Zeeb Road
Ann Arbor, Michigan 48106

THE USE OF A SELF-SCANNING SILICON PHOTODIODE ARRAY FOR ASTRONOMICAL SPECTROSCOPY

by

John Charles Geary

A Dissertation Submitted to the Faculty of the

DEPARTMENT OF ASTRONOMY

In Partial Fulfillment of the Requirements
For the Degree of

DOCTOR OF PHILOSOPHY

In the Graduate College

THE UNIVERSITY OF ARIZONA

1 9 7 5

THE UNIVERSITY OF ARIZONA

GRADUATE COLLEGE

I hereby recommend that this dissertation prepared under my direction by John Charles Geary

entitled THE USE OF A SELF-SCANNING SILICON PHOTODIODE ARRAY FOR ASTRONOMICAL SPECTROSCOPY

be accepted as fulfilling the dissertation requirement of the degree of Doctor of Philosophy

Nicholas Wallace — Dissertation Director

8/29/75 — Date

After inspection of the final copy of the dissertation, the following members of the Final Examination Committee concur in its approval and recommend its acceptance:*

J. R. P. Angel	8/29/75
R. B. Hilliard	8/29/75
P. A. Strittmatter	8/29/75

*This approval and acceptance is contingent on the candidate's adequate performance and defense of this dissertation at the final oral examination. The inclusion of this sheet bound into the library copy of the dissertation is evidence of satisfactory performance at the final examination.

STATEMENT BY AUTHOR

This dissertation has been submitted in partial fulfillment of requirements for an advanced degree at The University of Arizona and is deposited in the University Library to be made available to borrowers under rules of the Library.

Brief quotations from this dissertation are allowable without special permission, provided that accurate acknowledgment of source is made. Requests for permission for extended quotation from or reproduction of this manuscript in whole or in part may be granted by the head of the major department or the Dean of the Graduate College when in his judgment the proposed use of the material is in the interests of scholarship. In all other instances, however, permission must be obtained from the author.

SIGNED: John C Geary

ACKNOWLEDGMENTS

I wish to extend my appreciation to the following persons: Dr. G. R. Gilbert for serving as dissertation director and for continual support and encouragement; Drs. P. A. Strittmatter, J. R. P. Angel, and H. L. Hilliard for their informative and timely assistance during this investigation; Mr. J. Palmer for providing the absolute calibration for the radiometer used; Mr. T. Sargent for his many hours of assistance in assembling the computer software; and my wife Christraud, for her willing assistance in typing the drafts for this work.

Acknowledgment is gratefully extended to Dr. F. Low for the loan of the dewar container, to Dr. E. Snow and associates at the Reticon Corporation for the loan of the RL-128L photodiode array itself, and to Dr. W. Hoffman and colleagues for the use of many pieces of equipment during the course of this investigation.

TABLE OF CONTENTS

TABLE OF CONTENTS--Continued

LIST OF ILLUSTRATIONS

LIST OF ILLUSTRATIONS--Continued

ABSTRACT

The Reticon RL-128L self-scanning photodiode array is evaluated as a detector for astronomical spectroscopy. The utility and characteristics of this type of detector are discussed in relation to the physical processes involved and a detailed laboratory investigation presented, in addition to a final evaluation of a complete detector system at the telescope.

It was found that cooling to below a temperature of 150°K or so would be necessary for work on faint objects ($m_v \sim$ 12 or greater). Using a dewar container filled with liquid nitrogen, successful operation with no measurable dark leakage current has been demonstrated, even for integration intervals of several hours. However, an unavoidable loss in infrared response is introduced as a consequence of this degree of cooling, a situation to be avoided if the observational problem and physical design permits.

Absolute quantum efficiency was found to peak at approximately 83 percent, with a significant interference pattern modulating the overall sensitivity versus wavelength curve. The interference effect has been traced to the presence of a thin SiO_2 overcoating on the illuminated front surface of the array. This modulation has a large enough free spectral range that it can be easily calibrated out of the final spectral records, in addition to other diode-to-diode sensitivity variations.

Interference arising from reflection off the backside of the silicon substrate is neither expected nor observed.

With the signal fully digitized and the data acquisition process computer controlled, a dynamic range of better than 1000 has been achieved, with essentially complete linearity throughout. This, however, represents only about 10 percent of the dynamic range of the detector itself, indicating that more advanced designs may yield a system having a dynamic range in excess of 10^4.

The rather high noise level for this type of detector system at present limits its usefulness to objects of moderate brightness. However, within this constraint, such a detector system offers many important features, including high quantum efficiency, complete linearity, broad dynamic range and spectral sensitivity, and ease of data reduction, even when hundreds or indeed thousands of spectral records are involved.

CHAPTER I

INTRODUCTION

The importance of integrated silicon photodiode arrays for astronomical observations is linked to several properties of such devices which can produce a detector system of considerable power and flexibility. Of primary interest, perhaps, is the very high quantum efficiency of silicon over a spectral range extending from the near UV into the near IR, with advertised values for commercially available devices typically peaking at above 80 percent near 7500 Å. This figure may be compared to the quantum efficiencies for unsensitized photographic plates of 0.1 percent to 1.0 percent (Jones 1958; Zweig, Higgins, and MacAdam 1958) in the blue spectral region and perhaps a factor of 10 less in the near IR and to the quantum efficiencies of photoemissive surfaces of perhaps 25 percent in the blue and a few percent in the near IR.

Also of interest for astronomical observations are such factors as linearity, dynamic range, spatial resolution, and reproducibility of calibrations. The photogeneration of charges in semiconductors such as silicon is linear over a wide dynamic range with respect to incident illumination. This property can be preserved in commercially available devices if steps are taken to eliminate such nonlinear processes as leakage due to thermal generation of charge in the photodiodes. The dynamic range is a function of the total charge capacity of the photodiodes, the overall system noise, and the amplitude range of the signal

less than 100. Finally, extracting photometric data in quantitative form from a photographic record can introduce systematic errors, depending on the accuracy of the sensitometry and the methods employed by the researcher, and tends to be very tedious and time-consuming.

When coupled to an image tube, the effective quantum efficiency of the photographic plate is increased but with some degradation in resolution, and often troublesome spatial irregularities are introduced because of image tube distortions, photocathode nonuniformities, and nonuniformities in the output phosphors and optical couplers (Cromwell 1969; Cromwell and Dyvig 1973). While the output characteristics of the photocathode itself may be linear, the photographic record remains nonlinear and many of the problem areas mentioned above still remain. When used in a direct electron bombardment mode, the photographic plate becomes much more linear in its response and dynamic range can be greatly increased through the use of fine-grained emulsions, but data extraction remains a problem. Also, these latter devices have proved to be fragile and cumbersome to operate, and their use has not become widespread in astronomy for these reasons.

The development of various spectrum scanners employing photoelectric tubes capable of resolving individual photoelectrons has provided the astronomer a tool possessing high quantum efficiency, completely linear response, and dynamic range limited only by the signal processing and digital storage facilities. The price paid for these improvements has been the loss of multiplexing capability, a situation only partially alleviated through the use of multiple channels. In

practice, this restriction results in increased observing time or a corresponding decrease in resolution and spectral coverage, since each phototube can look at only one spectral element at a time. The introduction of image dissectors (Robinson and Wampler 1972), intensifiers utilizing wired diodes (Beaver 1973), and various television systems (Lowrance 1973; Boksenberg 1970; Gilbert 1973, 1975) represent attempts to retain the advantages of photoelectron counting while multiplexing the available information over a one-dimensional or full two-dimensional format. While such devices have recently produced results of great import, especially for the very faintest detectable sources, their general use in astronomy has been severely limited by the high cost in money and manpower necessary to build and successfully utilize them.

The use of a linear integrated photodiode array in an unintensified mode in the present investigation is an effort to produce a line-scanner for spectroscopy with performance characteristics significantly better than unaided photographic plates or even image tubes for some problems. Because photodiodes are inherently unity-gain devices at best, they cannot compete with intensified photoelectron-counting systems for use on faint objects due to the high overall system noise. However, on objects of moderate brightness, they offer immense advantages over the direct photographic plate and several distinct advantages over image tubes in doing accurate spectroscopic work, especially in the red and near IR spectral regions.

Photoelectric Properties of Silicon Diodes

In order to understand the nature of many of the observed performance characteristics, it is necessary to know some of the details of photogeneration and thermal generation processes in silicon semiconductors. Only those features that bear directly on this investigation are presented here. For more detailed discussions of these processes, the reader is referred to the books by Moss (1959), Bube (1960), and Ambroziak (1968).

Energy Bands and Excitation Processes

Whether energy is supplied by incident photons or internal thermal motions, the primary absorption process in silicon for this energy involves the excitation of an electron from the valence band to the conduction band, where it is then free to move through the processes of drift and diffusion. The energy necessary to make the transition from the maximum of the valence band to the minimum of the conduction band is defined as the band gap energy E_G and equals approximately 1.09 eV at 290°K for silicon. For several semiconductors, including silicon, the minimum energy in the conduction band does not lie at the same value of the momentum quantum number, k, as the maximum of the valence band. Conserving momentum for the incident photon and excited electron indicates that $\Delta k = 0$ represents the favored transition, called the direct transition. However, since the minimum energy transition requires a final $\Delta k \neq 0$, the actual favored process involves a direct excitation with $\Delta k = 0$ and a concurrent emission or absorption of a phonon, conserving both energy and momentum. There also exists the possibility of

a transition from the maximum of the valence band to the minimum of the conduction band without recourse to phonon absorption or emission. Since $\Delta k \neq 0$ for this transition, it is of lower probability and is called an indirect transition. For silicon, the probability for an indirect transition is typically 100 to 1000 times lower than that for a direct transition except at energies approaching the band gap energy. Finally, for photon energies in excess of 2.5 eV, a direct transition to the secondary minimum at $\Delta k = 0$ is possible. These excitation processes are illustrated in Figures 1 and 2, after Bube (1960).

Absorption Coefficients

For photons of energy greater than E_G, the direct transition process is highly efficient and is therefore reflected in a high absorption coefficient, illustrated in Figure 3 after Dash and Newman (1955). For incident radiation in the visible and near IR, the absorption coefficient approaches 10^5/cm, falling to below 10^2/cm for photons near the limit $h\nu = E_G$. Thus, the average penetration depth into a silicon substrate varies from a fraction of a micron in the blue spectral region to tens of microns in the near IR. The importance of this penetration depth for both the overall quantum efficiency of a silicon photodiode and the spatial resolution of an integrated photodiode array will be shown later.

Photodetection in a Reverse-Biased Diode

If a diode such as the one illustrated in Figure 4 is reverse-biased and then open-circuited, a quantity of charge is stored by the

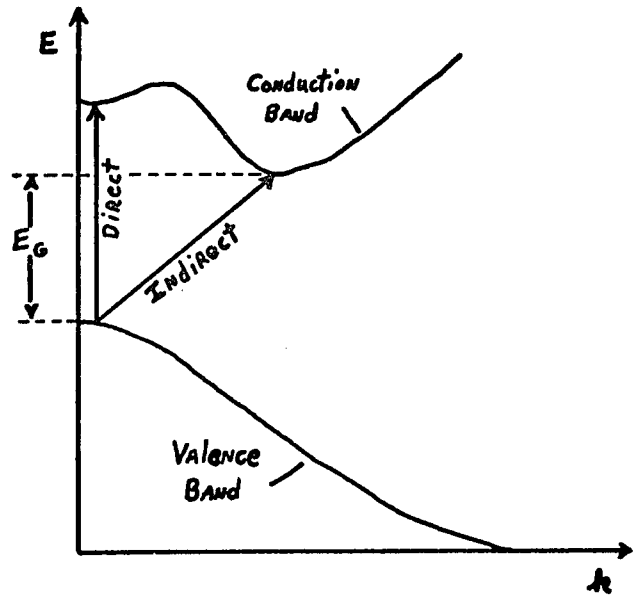

Fig. 1. Direct and Indirect Transitions in Silicon.

Direct transisions are made with $\Delta k = 0$; indirect transitions require $\Delta k \neq 0$.

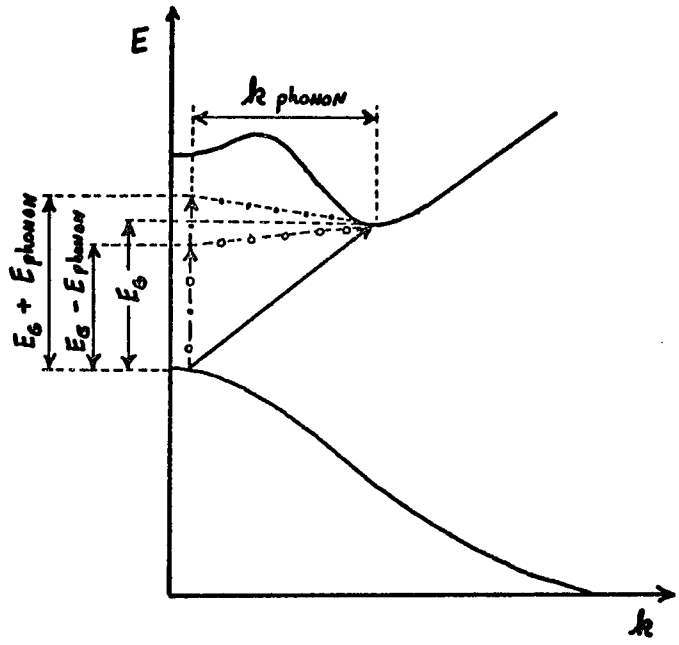

Fig. 2. Indirect Transition via a Favored Direct Transition with Concurrent Phonon Emission or Absorption.

The emission or absorption of a phonon allows conservation of both energy and momentum.

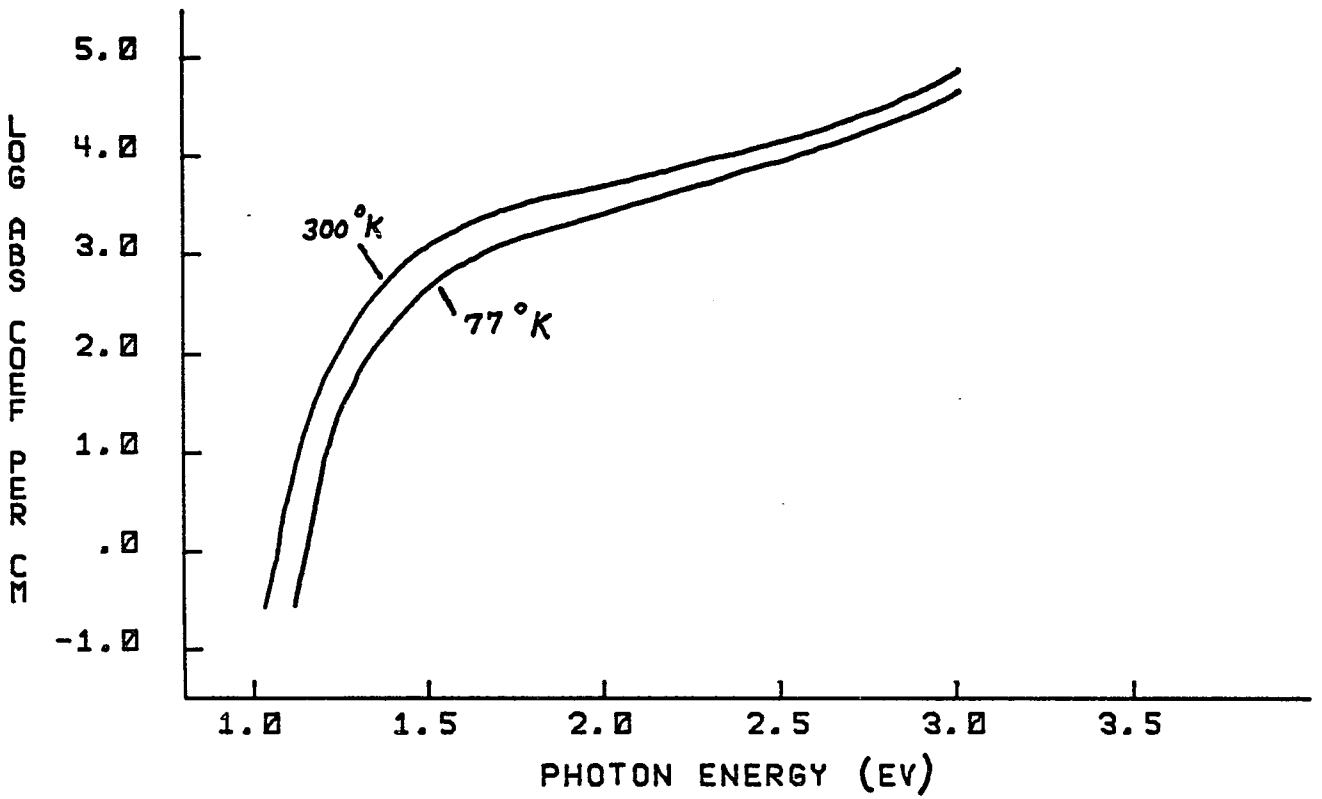

Fig. 3. Absorption Coefficient for Silicon versus Photon Energy

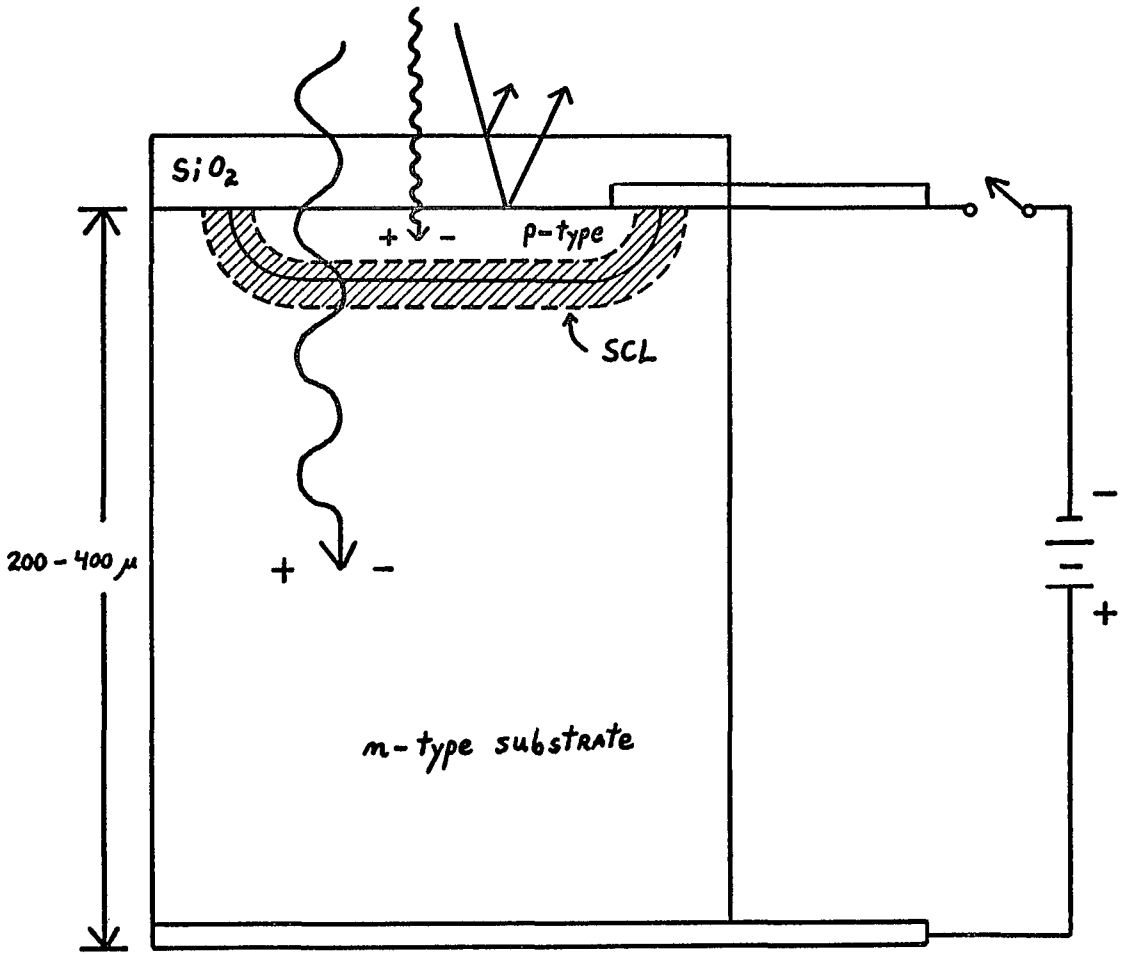

Fig. 4. Reverse-Biased Photodiode with Deep Substrate (Not to Scale).

Absorption of red and blue photons is illustrated, along with the possibility of front-surface interference effects.

junction due to the increased volume of the space-charge layer caused by the biasing voltage. The magnitude of this charge for an abrupt junction is given by:

$$\Delta q = A \left[2 q \varepsilon \frac{|(-V)|}{(1/N_D + 1/N_A)} \right]^{1/2} \quad (1)$$

where A is the junction area, N_A and N_D are the acceptor and donor concentrations, and (-V) is the reverse-bias voltage applied.

The diode may then be discharged if free charges are generated, either by photon absorption or thermal processes. By reapplying the original reverse-biasing voltage and measuring the amount of current necessary to restore the initial condition, the amount of free charge generated during the open circuit condition is determined. Such a photodiode is said to be operating in the charge-integration mode.

For the diode illustrated in Figure 4, comprised of a deep n-type substrate with an abrupt junction and a thin transparent p-type channel to which one of the electrodes is attached, the nature of the mobile charges which discharges the junction and the transport mechanism depend on the depth at which an electron/hole pair is formed. Throughout much of the visible and near IR region of the spectrum, the absorption coefficient is low enough to allow photon penetration into the n-type substrate. The dominant mechanism for charge transport to the junction is then the diffusion of holes to the space-charge region. If the absorption coefficient is high, as is the case toward the blue and near UV, it is also possible to get charge generation in the thin p-type

layer or in the space-charge layer itself. In the former situation, electrons will move toward the junction by diffusion. In the latter case, the current flow of electrons and holes is dominated by the drift mechanism, but the effect on the discharge of the diode is the same.

Factors Affecting Quantum Efficiency

Since the diode illustrated in Figure 4 is very thick in comparison to typical depths of penetration for photons having energy much in excess of the cutoff $h\nu = E_G$, the quantum efficiency should approach 100 percent. The extent to which actual performance fails to attain this ideal can largely be ascribed to the following three factors:

a. Silicon has a very high index of refraction, around n = 3.9 in the visible region of the spectrum. Uncoated, it is therefore highly reflective, resulting in a net loss in quantum efficiency. The Fresnel formulae for reflection show that the reflectivity for unpolarized illumination at normal incidence from air or vacuum should be approximately 36 percent, using the formula:

$$R = \left(\frac{n_2 - n_1}{n_2 + n_1} \right)^2 \qquad (2)$$

where n_1 is the refractive index of the incident medium and n_2 is the refractive index of illuminated medium. This unfortunate circumstance is partially offset by the surface passivation layer usually deposited on the front surface of the photodiode, typically a layer of SiO_2 a few microns thick. However, its index of refraction (n = 1.45) is not ideal for an antireflection film. Applying Equation 2, it is evident that the

resultant front surface reflectivity is approximately 3.4 percent and the reflectivity of the silicon boundary is approximately 21 percent, with this latter value rising to about 22 percent when multiple reflections are taken into account. The free spectral range of modulations in the transmissivity caused by interference at the front surface will be hundreds of angstroms for SiO_2 coatings several microns thick.

b. Recombination rates at the surface of a semiconductor will in general be higher than in the bulk material itself. This increased recombination rate therefore decreases the net diffusion current toward the diode junction for charge carriers generated near the top surface. The closer to this surface that carrier generation takes place and the deeper the junction lies, the more pronounced this effect will be. For a given diode, therefore, one expects this loss to be manifested in a drop in sensitivity toward the blue and near UV, where the absorption coefficient is so high that photons penetrate only a fraction of a micron. Although various chemical treatments are applied to the silicon surface to combat these losses, the effect is usually present to a greater or lesser extent depending on the manufacturing processes.

c. Carriers generated deeper in the diode substrate than the diffusion length will also not be effective in discharging the junction since recombination will on the average occur before the carriers can diffuse to the space-charge layer. This effect manifests itself in a drop in sensitivity as the cutoff energy $h\nu = E_G$ is approached, thus producing a gradual rather than an abrupt absorption edge. Because of the critical effects of impurities and lattice defects on the magnitude

of the diffusion length, it is generally not possible to specify this value a priori for a particular device.

The combined effects of the above three processes can be expected to be seen in the overall sensitivity characteristics of a front-illuminated diode like that shown in Figure 4 and of integrated arrays of similar construction. Quantitative results of these effects for the actual device under consideration are presented in Chapter III.

Other Possible Interference Effects

It has recently become evident that silicon target (ST) vidicons exhibit severe interference effects when illuminated with monochromatic light (McCord and Bosel 1973; Title 1974). Because the effect is large with presently available tubes and because it is in practice impossible to unambiguously access individual diodes in the target, this interference is difficult to calibrate out and accurate spectroscopy is not easily accomplished. The cause of this difficulty is the thinness of the target diodes, made necessary by the back-illuminated mode of operation. Standard ST vidicons typically have target diodes about 10 μ thick, with a few tubes designed for increased IR response having 20 μ diodes. It is therefore evident that a significant portion of the incident illumination in the near IR, where the absorption coefficient falls below 10^3/cm, can penetrate the entire thickness of the target diodes and be reflected off the back surface to produce interference effects. Because of the high refractive index of silicon, even the presence of a fast optical beam does little to help, and the only solution for ST

vidicon problem appears to be the development of better antireflection coatings (Title 1974).

The fact that integrated diode arrays are front-illuminated and are fabricated on substrates hundreds of microns thick means that no significant interference effects of the type seen in ST vidicons are possible, at least in spectral regions where such devices are still useful as photodetectors. Even in spectral regions where the combined direct and indirect absorption coefficients fall as low as 100/cm, the attenuation factor for a double pass through a deep substrate is very large. At the same time, the sensitivity is rapidly dropping because typical diffusion lengths are generally much less than 100 μ for these devices. It is possible that interference effects might be seen very near the photon cutoff energy where the quantum efficiency is approaching zero. The free spectral range for any such interference would only be about 4 Å for a 300 μ substrate and the incident illumination must therefore be quite monochromatic in order for the effect to be seen, as may be the case for solar instrumentation operated very near the absorption cutoff. For work in spectral regions where the quantum efficiency is still high enough for work on fainter sources, no such interference effects are expected and none were seen in the present investigation.

Thermal Charge Generation

For a reverse-biased diode junction of area A, the saturation current I_s which flows is ideally given by:

$$I_s = A\ q\ n_i^2(T) \left[\frac{D_h}{N_D\ L_h} + \frac{D_e}{N_A\ L_e} \right] \tag{3}$$

where $n_i(T)$ is the intrinsic carrier concentration, D and L are diffusion parameter and diffusion length, respectively, and N_A and N_D are the acceptor and donor concentration. I_s is the current responsible for the spontaneous discharge of the diode in the absence of light and is commonly called the dark leakage current. Except for temperatures so low that the doping atoms fail to ionize, the only strong temperature dependence in Equation 3 is contained in $n_i^2(T)$, given by:

$$n_i^2(T) = K\ T^3\ e^{-E_{GO}/kT} \propto I_s \tag{4}$$

where K is a constant and E_{GO} is the band gap energy extrapolated to absolute zero, approximately equal to 1.21 eV.

This radical dependence of I_s with temperature will not be realized for an actual silicon diode because of the effects of surface leakage and carrier generation at recombination centers within the space-charge region. Even at room temperature, the deviation of the temperature dependence of I_s from that predicted by Equation 4 is pronounced in silicon diodes and the relation given below is often used to describe the actual behavior:

$$\frac{I_s(T)}{I_s(T_o)} = 2^{[(T-T_o)/\alpha]} \tag{5}$$

The quantity α will vary depending on diode construction and geometry; for small diodes with abrupt junctions, this quantity typically has a value of about 6°C. However, it is difficult to predict whether such a relation can be used for extrapolations over wide variations in temperature for a given device. A graph of such an extrapolation for a cooled photodiode is presented in Figure 5, along with the much steeper exponential behavior of an ideal diode as given by Equation 4.

Effect of Cooling on Photodiode Response

The dark leakage current at room temperature will completely discharge the open-circuited junction in a matter of a second or so and substantial cooling will be necessary if long integration times are to be realized. However, as indicated in Figure 3, there is a pronounced decrease in absorption coefficient with decreasing temperature. This can be understood as an effective increase in the band gap energy E_G with decreasing temperature, since the effective energy of the valence band is coupled to the thermal energy contained in the crystal lattice, raising it slightly. The experimental value for the resultant shift in the silicon absorption edge is given approximately by:

$$\frac{dE_G}{dT} = -4.0 \times 10^{-4} \text{ eV/°K} \qquad (6)$$

as determined by Fan, Shepherd, and Spitzer (1956). Thus, cooling a silicon photodiode by 200° would produce a loss of almost 1000 Å in IR response if this were the only effect in evidence.

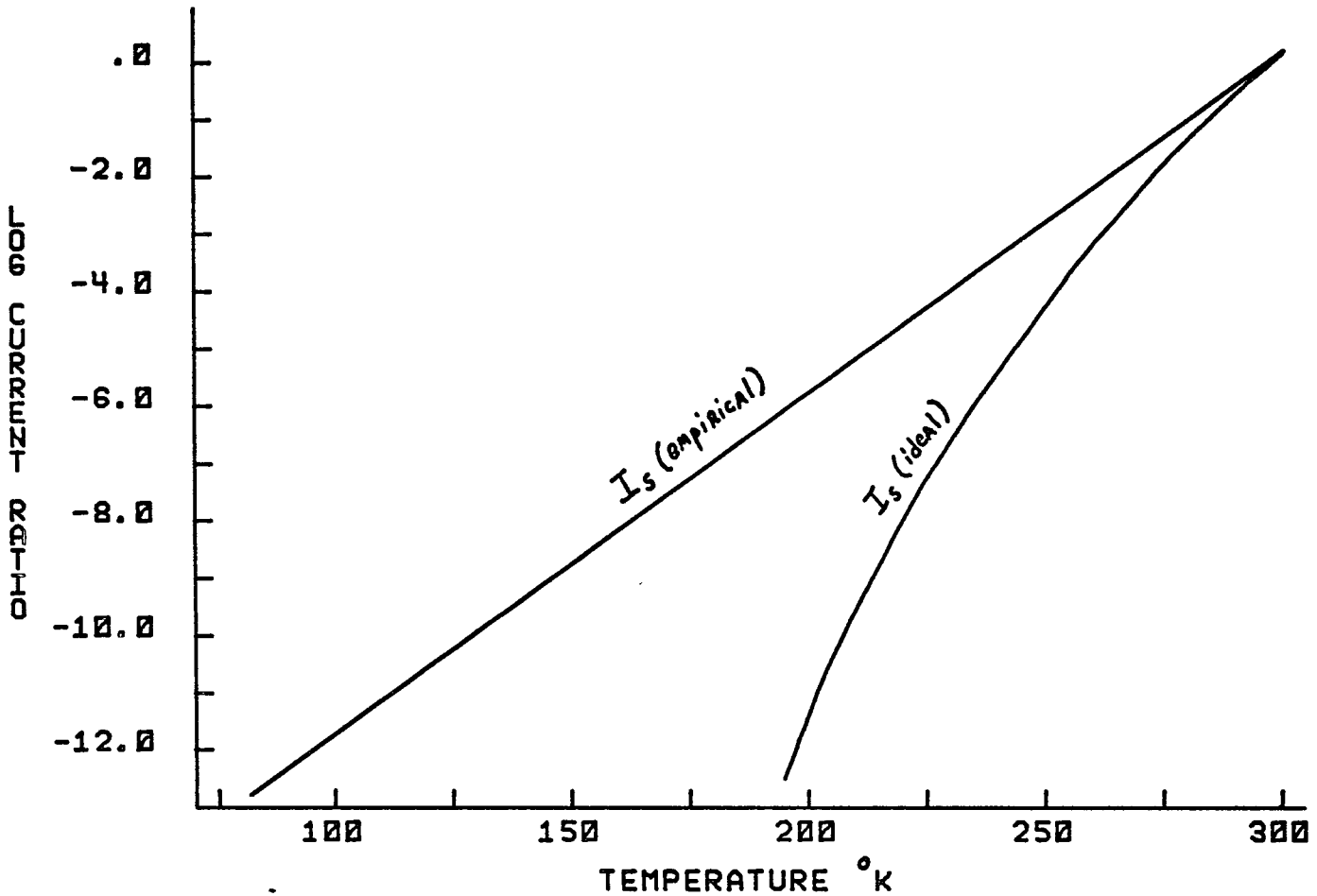

Fig. 5. Log [I_s (T)/I_s (300°K)] versus Temperature, Ideal and Empirical Behavior.

The actual situation for thick diodes is complicated by possible changes in the diffusion length. Again, because of the dominant role of impurities and lattice defects on this parameter, it is not possible to make a general prediction of the magnitude of this change for a particular device. However, one might expect the actual diffusion length to increase somewhat with decreasing temperature as carrier mobility increases and the effects of trapping centers perhaps decrease, thereby partially offsetting the increase in effective band gap and corresponding decrease in absorption coefficient.

Development of the Self-Scanning Integrated Photodiode Array

With the advent of the integrated circuit in the early 1960's, it was soon recognized that integrated imaging devices could be produced utilizing this technology. One of the first teams to attack the problem of producing not only an array of photosensors but also integrated scanning circuitry as well to access each element (Weimar et al. 1967) succeeded in making a 180 × 180 element phototransistor array utilizing thin-film integration techniques. Subsequently, interest quickly shifted to the newer metal oxide-silicon (MOS) technology because of the increased ease of fabrication and lower power requirements. Several devices, containing both phototransistor and photodiode sensing elements, were produced which demonstrated the feasibility of such detectors and led the way for eventual commercial production (Weckler 1967; Dyck and Weckler 1968; Noble 1968; Callahan and Torley 1968).

It was pointed out by Noble (1968) that photodiode arrays, while not producing the current gain of phototransistors, have a number of features which would make commercial production easier. These considerations in favor of photodiode arrays include smaller variations in sensitivity, lower leakage current, and production simplicity resulting in higher yields. It is perhaps unfortunate in a sense for applications involving detection at low light levels that these considerations proved to be overriding in the subsequent commercial development and refinement of this technology. In another sense, however, the present dominance of the integrated photodiode array is fortunate in that cooling to suppress the dark leakage current does not radically alter the output characteristics, as would probably be the case for phototransistor arrays designed for room temperature operation.

Previous Use of Integrated Photodiode Arrays in Astronomy

Because integrated photodiode arrays have only recently become commercially available, their use in astronomy is not yet well developed. The only published work concerning the use of such an array for direct imaging at the telescope (Tull and Nather 1973) dealt with the construction and testing of a low resolution spectrographic system. Although this effort did not attempt the ultimate in low noise performance, it served to demonstrate the potential of cooled photodiode arrays and to point out several design considerations and array parameters which directly affect its use for astronomical observations. In particular, the dramatic decrease in dark leakage current with cooling while still

maintaining satisfactory scanning operation was shown, along with the possibility of successful removal of switching transients from the digitized video signal. Efforts to adapt such devices to solar instrumentation have also proven successful (Livingston et al. 1975; Smithson 1975).

Several developmental efforts are also under way to use self-scanning photodiode arrays in conjunction with high-gain intensifiers in order to duplicate the photon-counting capability of image dissectors and wired-diode tubes. McNall (1973) proposes the use of a channel plate intensifier to produce the necessary gain, while Mende and Shelley (1975) indicate that photoelectron counting via direct bombardment of the diodes is feasible. Tull (1975) states that a self-scanning array has been successfully operated inside an image tube in a manner similar to the operation of wired-diode tubes. Photoelectron counting has proved to be possible with this device, but some radiation-induced damage eventually results. Finally, a self-scanning diode array has been successfully employed as an optical transducer for a high-resolution spectrograph for use in radio astronomy (Cole and Ables 1974) and as a detector for photographic reduction equipment (Høg and Wiskott 1974; Dravins 1975).

Characteristics of the Reticon RL-128L

Although self-scanning photodiode arrays are commercially available from several manufacturers, those of the Reticon Corporation have received the widest use in astronomy due to the broad range of sizes and options available. Because it was recognized at the beginning of this

investigation that cooling to quite low temperatures might be required, it was decided to use a new Reticon model containing low-power shift registers in order to reduce heating effects due to power dissipation on the array itself. Although the only available device at the time contained just 128 elements, it was felt that this would be entirely satisfactory to evaluate the overall performance characteristics of such devices and to accomplish spectroscopy of moderate resolution and coverage.

The Reticon RL-128L is a linear array of 128 square photodiodes on 63.5 μ centers. The diodes are accessed sequentially through FET gates driven by two parallel shift registers, one for odd and one for even elements, with the video pulses appearing on two separate output busses. Because the shift registers can be driven by two pairs of complementary clocks 180° out of phase with each other, the odd and even video pulses also share this phase relationship and the video output can then be multiplexed onto a single video line by simply tying the two outputs together. This then allows the use of a single preamplifier and eliminates the need for multiplexing in the subsequent circuitry.

Figure 6 depicts the analogous operation of the Reticon devices to the case of the reverse-biased diode discussed above. In the absence of a forward bias on the FET gates, the Reticon diodes are isolated from the video buss and can only be discharged by photocurrent or dark leakage current. When the scanning sequence is initiated in the shift registers by turning on the complementary clocks and providing the initializing start pulse, the FET gates are sequentially closed by application of a forward biasing pulse from the shift registers and then opened

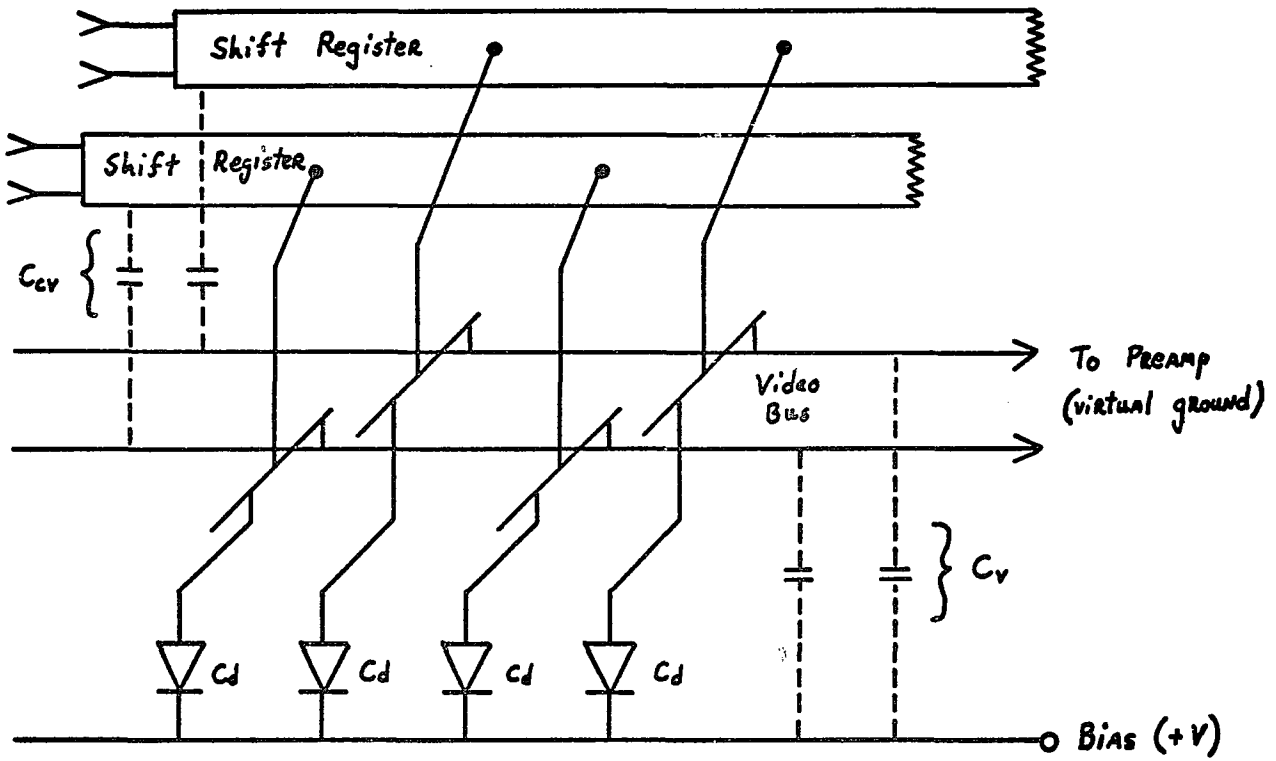

Fig. 6. Simplified Schematic of the Reticon RL-128L.

C_d is the diode charge storage capacitance. C_{cv} represents the parasitic capacitances of the gating switches and C_v is the total shunt capacitance of the output bus.

again after 1/4 clock period. During the time that the gate is closed, the diode is recharged to the bias potential, with current flowing from the positive bias voltage source to the virtual ground provided by the preamplifier in the case illustrated. This current pulse should show a time constant $\tau = R_{on} C_d$ where R_{on} is the on-resistance of the FET gate and C_d is the incremental capacitance of the photodiode. As R_{on} for good FET switches is small ($\sim$200 Ω) and the diode capacitance about 4 pf, this current pulse will be of extremely short duration for a preamplifier of sufficient bandwidth to maintain a virtual ground. For a +5 V bias, the total charge stored in the diode junction is approximately 4 pcoul, or 2.5×10^7 electrons.

Concurrent with the appearance of the video current pulse on the output bus, coupling of the clock signals through the parasitic capacitance C_{cv} also occurs. To the extent that the clock transitions are strictly complementary in phase, risetime, and amplitude and to the extent that C_{cv} is the same for each phase and diode, these transients would cancel and no net signal would result. In actuality, none of these conditions hold precisely, and quite large switching transients are introduced onto the video bus. Because the effects of variations in C_{cv} for individual diodes are generally smaller than asymmetries in the coupling of the clock phases, these signals tend to form a pattern with a periodicity equal to the number of phases, in this case 4. For this reason, these transients are often termed fixed-pattern noise, although the pattern is neither precisely fixed, due to small diode-to-diode variations in C_{cv}, nor is it noise in the sense that it is

stochastic and cannot therefore be removed from the processed video signal. Subtraction of a dark scan from a scan with impressed video signal can successfully remove the magnitude of the switching transients, although some residual noise may remain over that of the preamplifier. Also, maintaining fast rise- and fall-times for the clock signals and individually adjusting their amplitudes can reduce the magnitude of the switching transients significantly. In practice, these techniques can drop the magnitude of the transients to about 2 percent of the saturation signal from the photodiodes, but further reduction has proved difficult.

Because the common video bus lines see the combined output capacitance of all output gates, the total shunt capacitance C_V for such devices is quite high. A preliminary determination of the combined shunt capacitance for both video lines in parallel, using a current-to-voltage op amp configuration with variable input impedance, showed it to be approximately 50 pf for the RL-128L, a value confirmed by Snow (1975). The presence of this rather high shunt capacitance is a significant source of noise for the overall system and, as will be seen in Chapter II, its value couples strongly with the time constants for the filter network necessary for optimal noise performance.

The physical construction of the RL-128L is illustrated in Figure 7. As pointed out previously, the fact that the substrate is very thick compared to typical penetration depths for photons in the visible and near IR effectively rules out any interference effects arising from reflections off the back surface, even if this surface proved to be

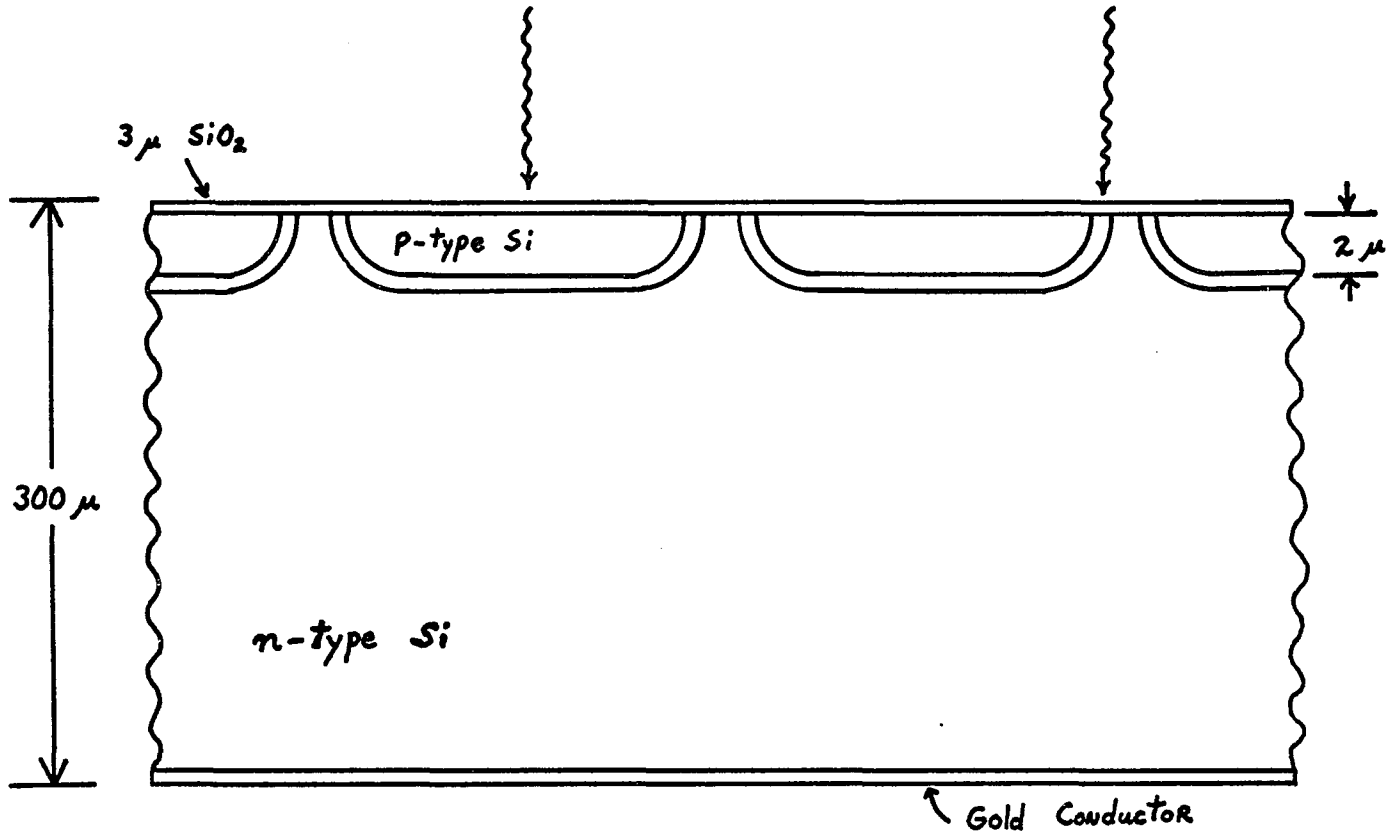

Fig. 7. Physical Construction of the RL-128L (Not to Scale).

plane reflector. Also, because the diode junctions lie only about 2 μ deep, surface effects are minimized and the response toward the blue should remain high. The surface of this device is coated with approximately 3 μ of SiO_2 and, thus, characteristic interference effects from this layer should be expected. As will be seen in Chapter IV, this effect can be removed by careful calibration of the individual diode responses versus wavelength for a given optical system.

CHAPTER II

INSTRUMENTAL DESIGN AND DEVELOPMENT

The degree to which a photodiode array such as the RL-128L must be cooled is directly related to the integration times necessary to produce acceptable signal-to-noise ratio (S/N). The noise in general will have components due to random variations in the array switching transients, electronic noise from the preamplifier, and shot noise from the dark leakage current in the diodes. By cooling the array sufficiently, one can effectively eliminate the noise contribution of the dark leakage current while at the same time allowing longer integration times, thereby building up enough signal to overcome the other two major noise sources. If possible, it is indeed desirable to reduce the average magnitude of the dark leakage current to a level far below that of the photocurrent being generated so that the need for multiple integrations to determine the leakage current at the time of observation is effectively eliminated.

For the RL-128L arrays, I found the dark leakage current at 295°K gives a 10 percent discharge of the diodes in 0.22 sec, or in terms of charge carriers, I_s (295°K) = 11.4 × 10^6 charges/(diode sec), as computed from the diode saturation charge given previously. Combined with the information in Figure 5, this value can be compared to the photon flux at the Cassegrain spectrograph focus of the Steward Observatory 90-inch (230 cm) telescope for typical objects to give an

indication of the amount of cooling necessary for a given astronomical problem. For a star of spectral type A0 and visual magnitude $m_v = 0$, the flux at the earth's surface is on the order of 1000 photons/ (cm^2 sec Å) at 5500 Å. Assuming that the efficiency for the entire optical system is on the order of 10 percent, this translates to a photon flux at the spectrograph focus of about 4×10^6 photons/ (sec Å diode) for the RL-128L with typical bandpasses of 2 to 5 Å/diode available with this spectrograph. Clearly, a significant amount of cooling is necessary to suppress the dark leakage current to a low level, even for such a bright source.

As mentioned in Chapter I, surface leakage and space-charge layer currents will produce anomolously high overall dark leakage, especially for a cooled diode, because of the lesser sensitivity to temperature than the exponentially varying volume thermal generation rate (Kleinknecht and Seiler 1954; Pell 1956). A test was conducted with the RL-128L in thermal contact with a reservoir containing dry ice (T = 195°K) in order to determine the validity of Equation 5. The equilibrium temperature of the mounting bracket for the array was measured to be 205°K using a forward-biased diode clamped in the same position as the array. The integration time necessary to produce a 10 percent discharge of the photodiodes was found to have increased by a factor of 65,000 from that determined at 295°K. The corresponding value of α is approximately 5.6°C, very close to the value typically found for good silicon diodes.

In order to more easily evaluate the amount of cooling required to carry out astronomical observations at low light levels, Figure 8 simultaneously displays photocurrent versus magnitude for the spectrograph focus and the extrapolated behavior of the dark leakage current as predicted by Equation 5, fitted to the experimental value above. Using this extrapolation then leads to the conclusion that for objects as faint as $m_v = 12.5$, cooling to temperatures below 150°K or so will be required in order to achieve the desired condition of negligible dark leakage compared to the signal available. However, three considerations must be kept in mind in choosing such as cooling system:

1. Whatever method is chosen should be able to maintain the array at a fairly constant temperature, not only to make any residual dark leakage current reproducible but also to maintain any other temperature-dependent output characteristics constant.

2. Lowering the temperature past the point sufficient to suppress the dark leakage current will produce an unwanted loss in quantum efficiency toward the red.

3. The array itself probably must be run in vacuum in order to prevent frosting and to insure uniform cooling.

One is therefore faced with either building a complex and expensive open- or closed-loop refrigeration system, capable of cooling to approximately 150°K, with active temperature control to maintain constant temperature, or using a simpler dewar chamber. Because of resource limitations, the latter course was chosen for the present investigation, although this choice puts some unfortunate mechanical and

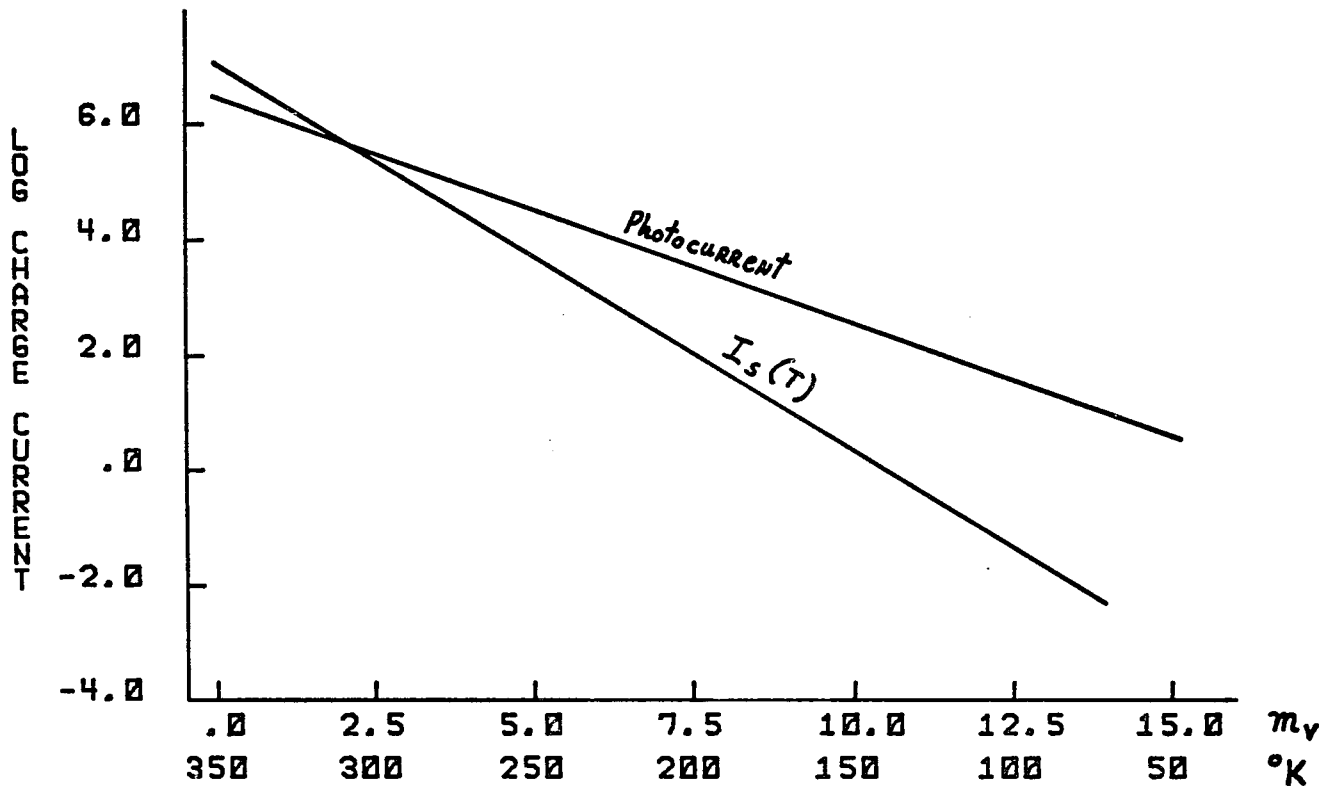

Fig. 8. Log I_s (T) versus Temperature and Log Photocurrent versus Magnitude for the 90" Cassegrain Spectrograph.

electronic constraints on the resultant system. In view of point 2 above, it would seem desirable to use a reservoir fluid which will maintain the array at temperatures of 150°K or so. There are several liquids which have freezing points in the right range but all have rather low specific heats and are flammable. Also, many dewar containers such as the one used in this investigation are designed for liquid nitrogen and therefore require a stream of cold gas from the reservoir to cool the internal radiation shield. When used with a nonvolatile slurry, the radiation shield of this type of dewar loses thermal contact with the reservoir and equilibrium conditions become difficult to maintain. After several attempts to use such frozen slurries in this type of dewar, it was found that a constant temperature could not be reliably maintained with such a configuration and liquid nitrogen (T = 77°K) was therefore used throughout the remainder of the program, with the subsequent loss in IR response unavoidably introduced. As a result, the measured quantum efficiency of the cooled array fell to only a few percent or less at wavelengths longer than 10,000 Å, making work in this spectral region impossible except for the brightest sources.

Care was taken at all times not to subject the array to gross thermal shock. The dewar was slowly cooled by dribbling small amounts of liquid nitrogen into the reservoir while monitoring the temperature of the baseplate with a forward-biased diode clamped to it for this purpose. A total cooling time of one and one-half hours or more produced no harmful effects in over 50 thermal cycles.

Having suppressed the magnitude of the dark leakage current to a level which is low in comparison to the photocurrent produced by objects of interest, the only time-dependent source of noise other than photon statistics is essentially eliminated. One is therefore free to integrate the available incident flux as long as desired within the limits of diode or electronic saturation. Since preamplifier noise and random noise in the switching transients are in principle unrelated to the integration time, averaging multiple scans of bright sources, integrated to near the saturation level, will improve the signal-to-noise ratio by the expected factor of $\sqrt{m}$, where m is the number of scans. However, on fainter sources where the total signal will not saturate the system within the total observing time, it is desirable to utilize the freedom available from cooling to make a single integration of the available signal rather than several scans. The latter situation would actually degrade the signal-to-noise ratio by the factor $\sqrt{m}$, since the total signal is fixed but the noise has been increased by this factor due to multiple readouts.

Dewar Design and Electronic Layout

A sectional drawing of the dewar, along with the orientation of detector, drive circuitry, and preamplifier is shown in Figure 9. The array itself is clamped to the reservoir by means of a solid copper block into which a machined recess allows it to be embedded. Thermal contact is assisted by the use of small amounts of vacuum silicone grease on the backside of the array package and on the baseplate interface. The array itself is without the normal quartz lid covering the

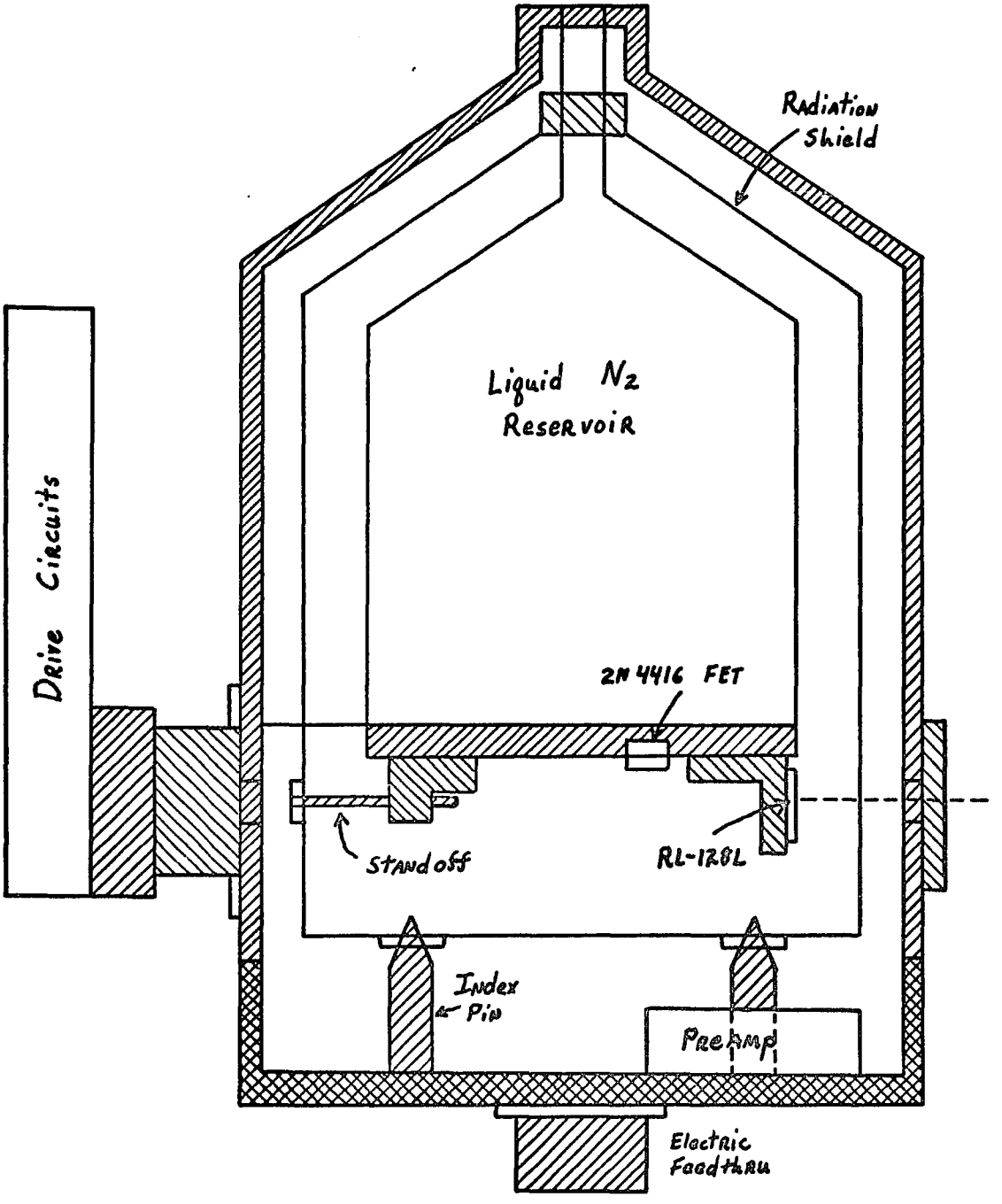

Fig. 9. Sectional Drawing of Dewar Container (Not to Scale).

top of the package. This not only eliminates potential problems with condensation, outgassing, and explosion in vacuum, but also eliminates a potential source of interference effects.

Because of the placement of the electrical feedthrough port, it was necessary to bring the clock signals to the RL-128L across a linear distance of approximately 15 cm. The alternative to this arrangement would be to mount the MOS clock drivers close to the array itself, operating in vacuum. However, since power dissipation in the drivers is quite high, it was decided to mount them external to the vacuum wall. Although the resulting long coaxial clock lines may couple the clock transients more strongly to the preamplifier, the effect does not appear to be large. However, the introduction of random noise is certainly possible with this arrangement and the shortening of such clock lines is probably desirable if the mechanical layout permits.

The preamplifier chosen dissipates most of its power in the input FET stage and it therefore proved possible to place it entirely inside the vacuum chamber. This arrangement allows the thick dewar wall to act as both an electromagnetic shield and as a massive ground reference for the entire system, thereby eliminating potential problems related to the noise pickup and the effects of ground loops. To accommodate the preamplifier board, a deep baseplate was machined for the dewar. Mounted in this baseplate are two large steel pins which serve to locate the radiation shield, which in turn is tied to the inner reservoir through short kel-F standoffs. These components were made as short and as strong as possible in order to minimize flexure within the

dewar itself. Although these heavy standoffs and index pins tend to increase thermal conductivity into the dewar, with a high resultant consumption rate of liquid nitrogen, they are absolutely essential in order to maintain mechanical stability in the focal plane of the camera. With the entire system powered up, hold time for the 2-liter dewar reservoir was more than seven hours, an acceptable level for telescope operation.

Preamplifier/Filter Design Considerations

Because of the critical effect of electronic noise on overall performance of a unity-gain device like a photodiode array, care must be taken to minimize it throughout the system. The most critical point is the preamplifier, since it will generally be the highest-gain stage. Analysis of the design parameters for low-noise preamplifiers is fortunately well developed although ideal performance often remains elusive in actual systems. The discussion below of the design parameters of a preamplifier suitable for the RL-128L follows earlier treatments of the general problem by Goulding (1966).

To first approximation, the recharging of the array photodiodes can be modelled as an ideal current source for the subsequent preamplifier stage. This, coupled with the desirability of reducing preamplifier sensitivity to total shunt capacitance, indicates that an integrating, or charge-sensitive, preamplifier design will probably be optimal in achieving the best noise performance. A diagram of such a charge-sensitive preamplifier and a noise model for this configuration are presented in Figure 10. C is the total shunt capacitance to ground, the sum of the diode capacitance, detector shunt capacitance, input

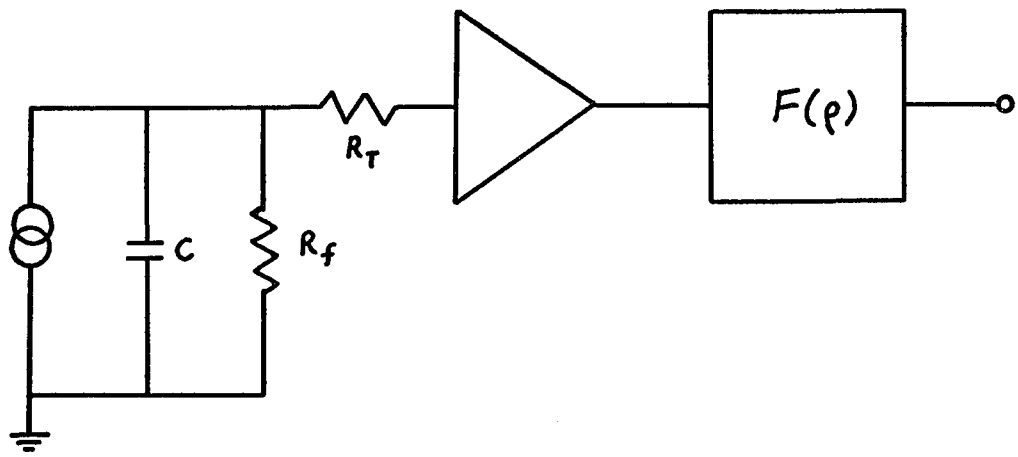

Fig. 10. Preamplifier Noise Model.

capacitance of the preamplifier, and the integrating feedback capacitor. In the case of the RL-128L and similar devices, detector shunt capacitance is large compared to the others. R_f is the feedback resistor of the integrating preamplifier and R_T is the equivalent noise resistance of the input stage of the preamplifier, given by Equation 7 in the case of a good JFET, after van der Ziel (1962).

$$R_T = 0.7/g_m \tag{7}$$

The noise voltage contributions from R_T and R_f are, respectively:

$$dv_{TM}^2 = 4\ k\ T\ R_T\ df \tag{8}$$

$$dv_{fM}^2 = \frac{4\ k\ T}{R_f\ \omega^2\ c^2}\ df \tag{9}$$

The role of the filter stage in Figure 10 will be to maximize the amount of signal passed through while blocking as much noise as possible. For a charge q introduced at the preamplifier input, the peak signal voltage at the output of the filter will be:

$$S = P\left(\frac{q}{C_f}\right) \tag{10}$$

where P is the transfer coefficient of the filter network and C_f is the integrating feedback capacitor. For a filter network having a characteristic frequency f_o and an overall filter function $F(\rho)$, where $\rho = f/f_o$, Equations 9 and 10 then give the differential noise-to-signal ratios:

$$\frac{dv_{TM}^2}{S^2} = \frac{4\ k\ T\ R_T\ C^2\ f_o}{P^2\ q^2}\ d\rho \tag{11}$$

$$\frac{dv_{fM}^2}{S^2} = \frac{k\ T}{\pi^2\ P^2\ q^2\ R_f\ f_o}\ \frac{d\rho}{\rho^2} \tag{12}$$

Weighting by $F(\rho)$ and integrating over all frequencies then gives:

$$\frac{v_{TM}^2}{S^2} = \left(\frac{4\ k\ T}{P^2\ q^2}\right) R_T\ C^2\ f_o \int_o^\infty F^2(\rho)\ d\rho \tag{13}$$

$$\frac{v_{fM}^2}{S^2} = \left(\frac{k\ T}{\pi^2\ P^2\ q^2}\right) \frac{1}{R_f\ f_o} \int_o^\infty F^2(\rho)\ \frac{d\rho}{\rho^2} \tag{14}$$

The sum of these two ratios will evidently have a minimum value at some f_o which depends slightly on the filter function $F(\rho)$ because of the integrals above. Ignoring this latter effect for the moment, a noise-corner frequency f_{nc} can be defined as the value of f_o which minimizes the sum of the coefficients of Equations 13 and 14, giving:

$$f_{nc} = (2\ \pi\ C\ \sqrt{R_T\ R_f})^{-1} \tag{15}$$

The total mean-square noise to signal ratio can then be expressed as:

$$\frac{v_n^2}{S^2} = \left(\frac{k\ T}{\pi^2\ P^2\ q^2}\right) \frac{1}{R_f\ f_{nc}} \left[\frac{f_o}{f_{nc}}\ I_T + \frac{f_{nc}}{f_o}\ I_f\right] \tag{16}$$

where I_T and I_f are the integrals in Equations 13 and 14, respectively. The optimal filter frequency f_o which minimizes the quantity in brackets can then be found by setting the two terms equal, or:

$$\frac{f_o}{f_{nc}} = \frac{I_f}{I_T} \tag{17}$$

The bandwidth integrals I_T and I_f can be evaluated once the form of the filter network is chosen, and f_{nc} can be computed from the parameters of the detector and preamplifier, thus yielding the value of f_o for the filter to optimize the signal to noise ratio for the system. The most common approach for an integrating charge-sensitive preamplifier is to differentiate the output in the first filter stage, with one or more RC integrations following, all with the same time constant as determined by f_o. Hunten (1972) has analyzed this type of filter network and concludes that little can be gained in performance by introducing more than two stages of integration following the differentiation. For this particular case, the evaluation of the bandwidth integrals in Equation 17 then gives:

$$\frac{f_o}{f_{nc}} = \sqrt{3} \tag{18}$$

The quantity in brackets in Equation 16 is then $\pi\sqrt{3}/8$ and P is 0.271, thus allowing the quantity v_n^2/S^2 to be evaluated for a given detector and preamplifier configuration. This expression has dimensions of $(\text{charge})^2$, and it is customary to refer to the square root of this quantity as the equivalent noise charge referred to the input of the preamplifier, or ENC.

The above filter configuration requires that the time constant for the integrating preamplifier is long compared to the interval between pulses, thus producing a step-function at the input of the

differentiating stage. Unless the slew range of the preamplifier is very large, however, such an arrangement will severely limit the dynamic range of the system because of saturation in the preamplifier itself. For reasons of size and power dissipation, it was decided to use a preamplifier design of moderate voltage range for this investigation, therefore necessitating a rather short feedback time constant in order to preserve dynamic range, a situation compounded by the inability of this particular array to operate reliably at scanning rates much below 8 kHz when cooled. The actual values chosen for the preamplifier feedback loop were a 1 pf integrating capacitor (C_f) shunted by a 192 M Eltec miniature resistor (R_f), producing a time constant of 192 μsec.

An undesirable undershoot would result if this signal were differentiated by a simple RC stage, and a pole-zero cancellation (PZC) network was therefore utilized as the first stage of the filter. This not only performs the initial differentiation and eliminates any undershoot but also can produce a pulse of the desired time constant $\tau_o = (2 \pi f_o)^{-1}$ if component values are properly chosen. The diagram of a PZC network is shown in Appendix A along with the relations necessary to determine the required component values to match the input and output time constants.

Using the equations developed above and the output parameters of the RL-128L array, the value of f_o to be incorporated in the filter network and the theoretical ENC for the resultant system can be computed. As mentioned in Chapter I, the shunt capacitance C_v for the array is approximately 50 pf, a large value compared to both the input capacitance

of a good JFET and the 1 pf integrating capacitor C_f. The value 50 pf will therefore be used throughout the succeeding discussion for C, the total noise capacitance of the detector/preamplifier system. For the dewar configuration used in this study, cooling of the input JFET is desirable, both to increase g_m and thereby decrease R_T and also to insure a safe and stable operating temperature in vacuum. While g_m typically reaches a maximum around 130°K, it still remains high even at liquid nitrogen temperatures. A TI 2N4416 JFET was chosen for this purpose because it offers good noise performance with low input capacitance and has been extensively studied in low temperature applications (Aitkin 1968; Goulding, Walton, and Pehl, 1970). The measured value of g_m for the transistor chosen was 12.5 mmhos at 77°K, yielding a value of 56 Ω for R_T from Equation 7. Substituting this and the values for C and R_f into the equations developed above will then give the following values for the system:

$$f_{nc} = 30.9 \text{ kHz}$$

$$f_o = 53.5 \text{ kHz}$$

$$\text{ENC} = 80.1 \text{ e}^-$$

With f_o now known, the design of the filter network can be completed. Actual component values will depend on the drive capabilities and input considerations of the buffer amplifiers used in the filter network. Schematic drawings of the complete preamplifier and filter network is presented in Appendices B and C.

The open loop gain of the preamplifier itself was measured to be approximately 82 dB, with a bandwidth between 3 dB points of 560 kHz. When connected to the RL-128L in its charge-sensitive configuration and with the filter network in place, the measured ENC was found to be approximately 890 e^-, a value considerably in excess of the theoretical value above. This is to be expected because of the less than ideal physical configuration of the preamplifier which is required by the present dewar arrangement. Also, much of the excess noise may result from leakage in the glass header of the 2N4416 JFET, an important effect at low temperature where the gate current drops to an extremely low value (Kern and McKenzie 1974).

Drive Circuitry and Switching Transients

The RL-128L array can be driven in either of two modes to produce full video output, as shown in Figures 11 and 12. The clock waveforms in Figure 11 have all transitions occuring in complementary pairs rather than being mixed over all four phases as depicted in Figure 12. Although one might therefore conclude that the magnitude of the resultant switching transients could better be nulled out by amplitude and phase adjustments using the former arrangement, in fact there seems to be little difference between the two schemes. For the sake of circuit simplicity and also to avoid any unwanted effects caused by the output video line being gated to two diodes simultaneously (as in Fig. 11), the driver scheme depicted in Figure 12 was chosen for the final version of the system.

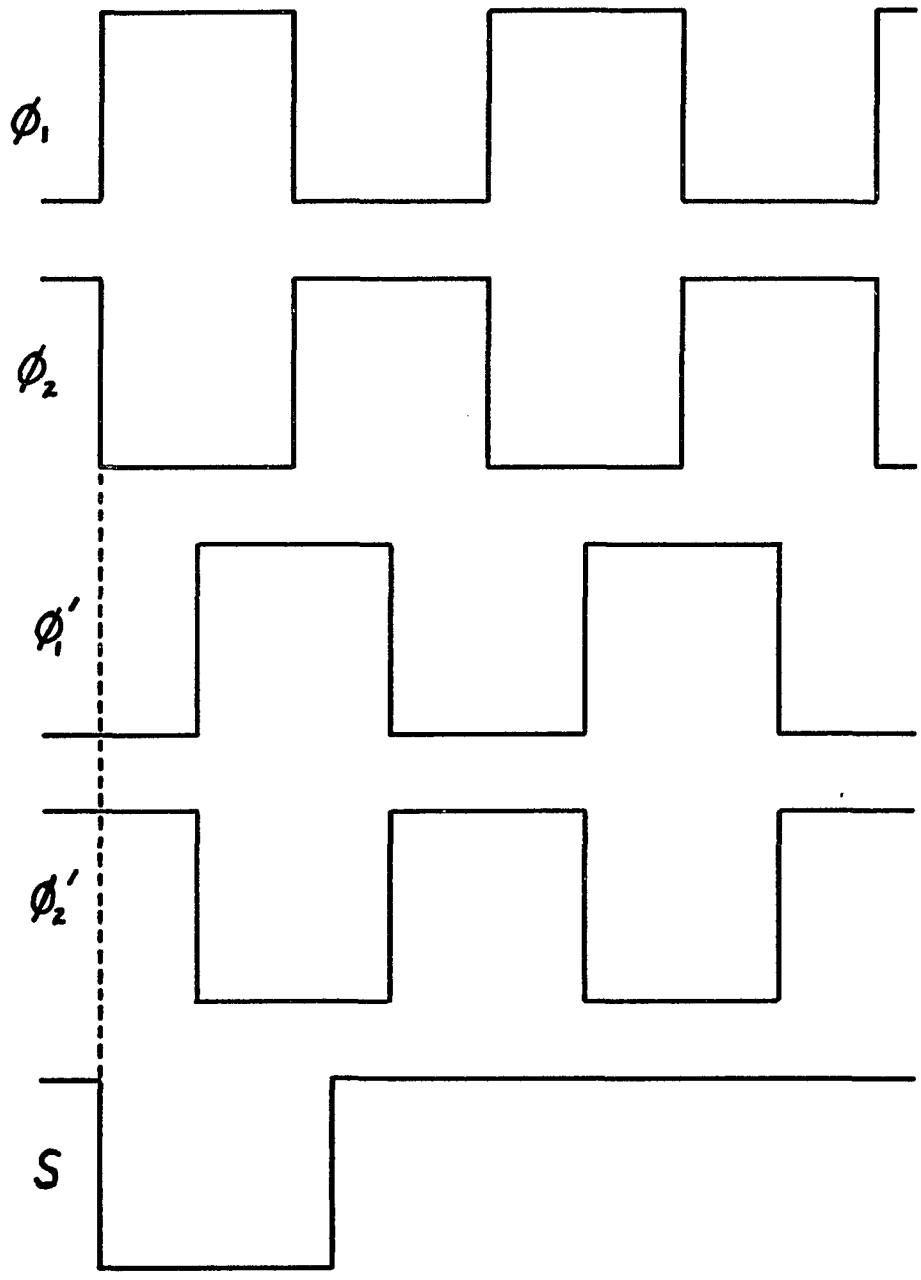

Fig. 11. Clock Waveforms (Complementary Pairs).

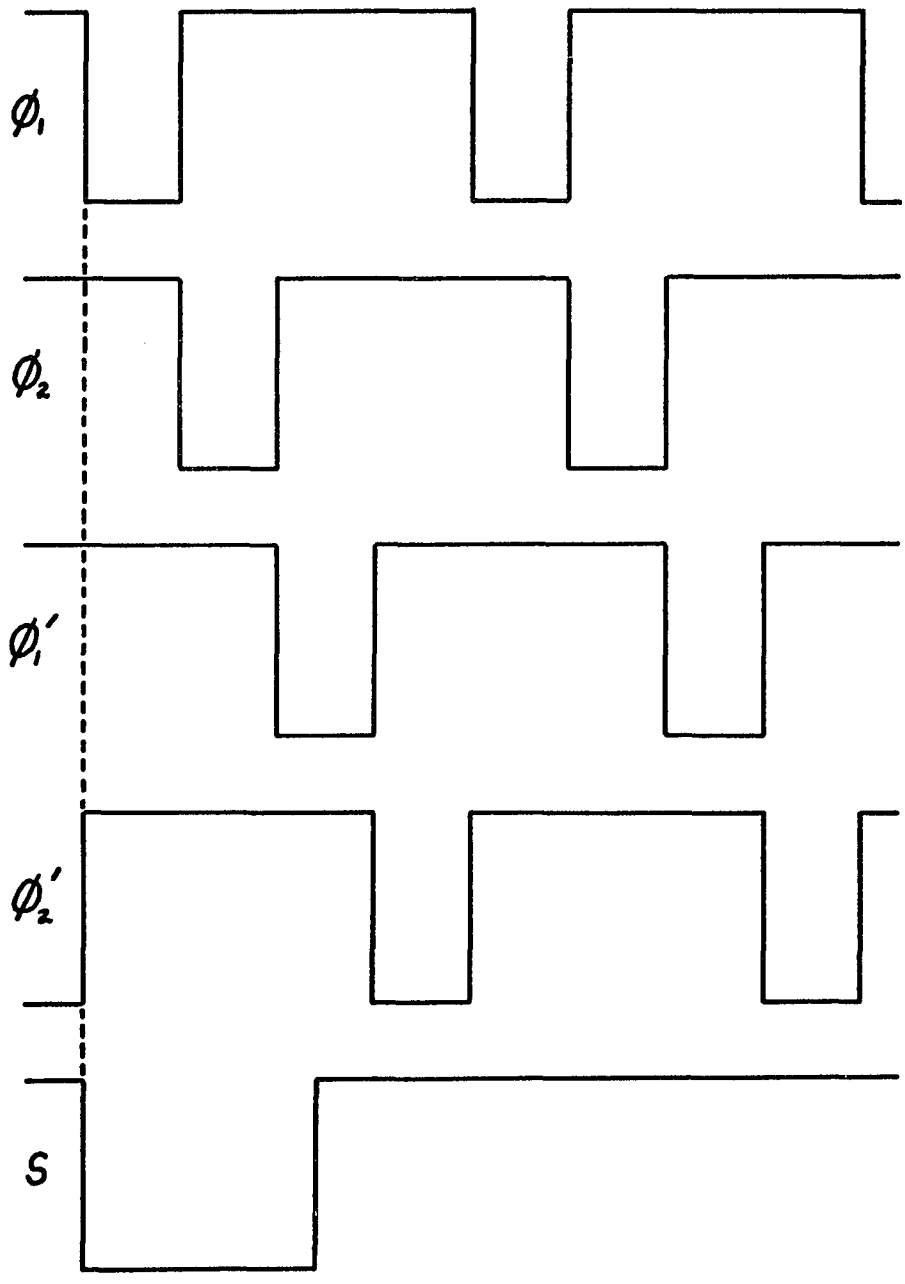

Fig. 12. Clock Waveforms (Noncomplementary Pairs).

As part of the overall system evaluation, several tests were conducted to ascertain what parameters influence the magnitude and form of the switching transients. All of these tests were performed with the array cooled so that the dark signal was eliminated from the video output. It was initially hoped that allowing complete freedom in both amplitude and relative phase between the four clocks could effectively reduce the magnitude of the transients to a low level. In addition, the effects of such variables as clock line length and shielding were investigated. The results of these tests are as follows:

a. To a point, shielding the output video pins and preamplifier can reduce the magnitude of the induced transients. However, once this level has been reduced to around 2 percent of the saturation signal of the diode array, further sophistication in shielding is ineffective in reducing the transients further, indicating that the residual effects are intrinsic to the array itself.

b. The switching transient appears essentially identical to the true video pulse and cannot be gated from the true output video signal to any extent. To the accuracy of the electronics used, the total video signal is a linear combination of the switching transient plus true video pulse, both with identical time constants and phase.

c. The adjustment of the phase relationship between complementary pairs of clocks proved unsuccessful in reducing the magnitude of the switching transients significantly. Since such efforts proved to be of marginal utility and because of the possible increase in noise on the

transients due to delay circuitry jitter, this adjustment capability was eliminated from the final version of the system.

d. Adjustment of the individual amplitude swings of each of the four clocks and adjustment of the overall DC level of all four clocks together proved to be effective in tuning to minimum switching transient output while maintaining full diode accessing. It was found that the +V supplier could be ganged together for all four clock drivers, with the -V supplies then individually variable. Best operation was obtained when +V was set slightly positive (0.1 V) with respect to the bias voltage for the array. Adjustment of the four -V supplies could then reduce the magnitude of the switching transients to about 1 percent of the diode saturation signal. Once set, the switching transient pattern across the array remains essentially invariant to the extent that temperature and preamplifier characteristics reamin constant. The clock generation circuitry and high speed MOS drivers are shown in Appendix D.

A/D Conversion and Computer Interface

After being amplified by the preamplifier and shaped by the filter network, the processed video pulse goes to a clocked sample-and-hold (S/H) module set to sample the peak of this pulse. The sensed level is then fed to an analog cancellation stage, followed by a final amplifier driving a 12-bit analog-to-digital (A/D) converter. The complete schematic for this section is shown in Appendix E. All of the TTL circuitry needed to gate the S/H and A/D modules is included on this board, along with a synchronous counter and buffer/driver gates to aid in interfacing with the computer. Various adjustable delays are built into the gating

circuitry to allow accurate peak-sampling of the video pulse and to provide sufficient settling time for the analog signals.

The purpose of the analog cancellation circuitry mentioned above is to allow subtraction of the approximate magnitude of the switching transients in real time so that most of the dynamic range of the A/D converter is available for the true video signal. This can be accomplished in a simple fashion in the case of the RL-128L, since the form of the transient pattern repeats cyclically with a period of four. Thus, a simple MOS switch circuit, gating appropriate DC levels from adjustable voltage dividers into one side of a differential amplifier, can null out much of the magnitude of the switching transients, upon which the true video signal is impressed. A residual pattern will still remain because of small diode-to-diode variations in the switching transients, but these can subsequently be removed through digital subtraction in the computer. As actually constructed, the analog cancellation circuitry does not appear to appreciably increase the overall system noise level and succeeds quite well in preserving the dynamic range of the A/D converter.

With much of the control logic already present in the drive and signal processing circuits, the actual interface to the Nova 800 computer can be accomplished with a single D-type flip-flop and a few driver and receiver gates. The interface is constructed on a general purpose DG 4040 board and is shown schematically in Appendix F. Pulses generated by the computer can both control the gating to the master clock for the array drive circuitry and generate the initializing start pulse to begin

the serial readout of the video signal. This scheme allows the programmer a great deal of freedom in controlling the timing of these events to tune the system for optimal performance.

Software

Both the control and data reduction programming has been done in the FORTH language, as modified and developed at Steward Observatory. For a device such as the RL-128L, producing data which is already serialized and spatially discrete, the basic scan cycle and data reduction are extremely simple. After the master clock for the drive and signal processing circuits is gated in and a start pulse generated to initiate the scan, the program awaits the arrival of the end-of-conversion (EOC) pulse from the A/D module and then reads the data word which has just been formed. In this way, all 128 data words are read into core memory and stored as a sequential array. For each integration on the RL-128L, two successive scans are made and the data stored in separate data arrays, one containing video signal plus residual switching transients and the second containing just the residual switching transients. After checking for overflow caused by saturation in the signal processing electronics, the second scan is subtracted from the first, leaving only the true video signal plus any noise which is present. Calibration factors may then be applied individually to each video element to produce output data representing true intensity for each diode. Various programs have also been developed to store and display this data, both for immediate access at the telescope for the observer's benefit and for

detailed processing at a later time to allow full correction for all instrumental effects.

Final System Configuration

The layout of the entire electronic system, as actually constructed and utilized for this investigation, is presented in block diagram form in Figure 13. Because of the high gain and low noise requirements on the complete system, the configuration of the gound lines between each segment is critical to the overall performance. It is essential that all grounds, including those of the external power supplies and the computer, derive from a single point. For this system, the point chosen is the aluminum case of the dewar container. Grounds to all components of the rest of the system then radiate individually from the dewar case, as shown in Figure 13. This configuration produced the lowest measured noise level for the entire system and was significantly better than other grounding layouts which were tried.

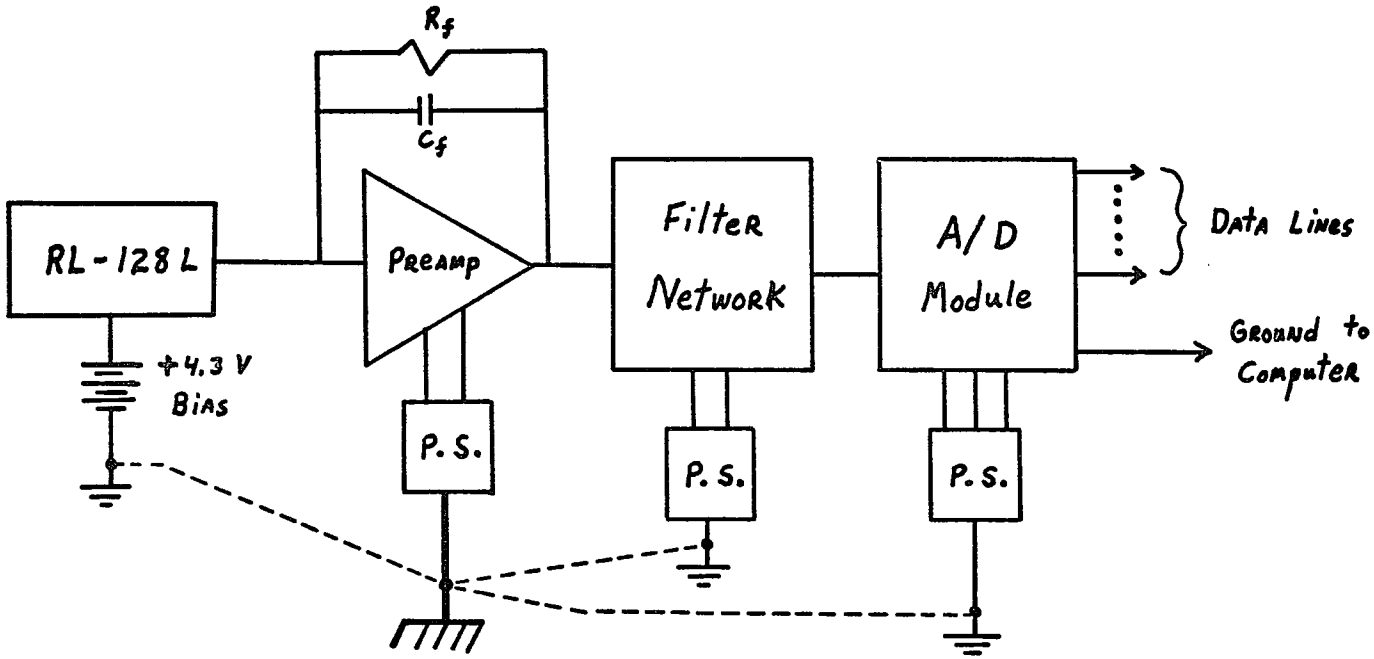

Fig. 13. System Block Diagram.

CHAPTER III

LABORATORY PERFORMANCE

System Noise

Evaluation of the overall system noise is readily accomplished once the data has been digitized and stored in the computer. The ultimate measure of this noise is determined by the extent to which the array switching transients, with any system noise impressed upon them, will cancel when two dark scans are subtracted. Thus, the distribution of the residuals from such a subtraction gives immediately the system noise which can then be expressed in terms of ENC when referenced back to the preamplifier input. Because of the low operating temperature for this system, dark current is not a factor in this determination, and the only noise sources remaining are preamplifier noise, random variations in the switching transients, and DC drift in the electronics.

While performing the tests on overall system noise, two effects were noted which should be considered in future designs, especially those utilizing a cooled preamplifier input. It was immediately evident that a considerable warm-up period, sometimes 30 minutes or more, must be provided before the preamplifier reaches equilibrium. This is probably due to the fact that the transconductance, g_m, is increasing slightly as the temperature of the JFET rises due to power dissipation. Also, because gate current is very low for a cooled JFET, some anomolous space-charge effects or thermal transients may occur in the junction

regions, producing a low frequency noise source (i.e., a DC drift) for scans separated by a time interval. After the warm-up period, the characteristics of the preamplifier and detector appeared to remain stable over periods of many hours.

The effects of the DC drift are of particular concern for long integrations, where the system clocks are turned off for a long period of time in order to insure that the array itself is not being heated appreciably. This drift appears in the digital output as a slightly negative result when the two scans of the scanning cycle are subtracted. Since tests of the A/D converter and associated electronics alone produced no such effects, this shift must be ascribed to the preamplifier stage. The only effective way of combating this drift appears to be through the use of a gating arrangement for the master clock and start pulses in order to provide a constant set of initial conditions for the scanning cycle. Thus, the system can be tuned for optimal noise performance by adjusting the time interval between the onset of the master clock, starting the MOS drivers which generate the 4-phase clock signals for the array shift registers, and the initiating start pulse which actually begins the scanning cycle. Best noise performance was obtained when the master clock was gated in approximately 0.5 sec. before the first scan was initiated, with the second scan to provide suppression of the switching transients initiated immediately after the first.

The measured value for the overall system noise, defined as the RMS variations in the output of any single element in the absence of light, was then found to correspond to a count of approximately 2.8 at

the output of the A/D converter. Referenced back to the input of the preamplifier, this corresponds to 4760 equivalent electrons, considerably in excess of the 890 e^- measured for the preamplifier alone. A test was therefore conducted in which the drive signals were removed from the RL-128L but the rest of the system left intact. Thus, the output of the A/D converter would reflect only noise contributions from the preamplifier and following stages. It was found that the noise level registered in this way was about half that for the operational configuration. Thus there exists a portion of the total noise that must be ascribed to the preamplifier/filter which is in excess of the high frequency noise seen on an oscilloscope. This can probably be ascribed to the characteristic 1/f noise found in many electronic systems. The remainder of the noise for the complete system must be ascribed to variations in the driving clock signals, producing noise on the switching transients. This effect remained troublesome despite efforts to regularize the clock signals through the use of a stabilized precision master clock. It is possible, however, that such approaches as redesign of the dewar container to allow closer positioning of the MOS clock drivers to the array and more massive power supplies for these drivers, preloaded to combat power transients caused by initiation of a scan, might be useful in reducing any excess noise introduced on the switching transients.

Linearity

The system linearity was measured by using a stabilized light source and then varying the signal by adjusting exposure times. It is

evident from these measurements that, to within the limits of experimental error imposed by electronic noise and the stability of the light source, the RL-128L is completely linear over the dynamic range allowed by the system electronics, about 10 percent of the saturation level of the diode elements. This statement holds true for both the array average and for individual diode elements, although diode-to-diode variations in sensitivity are quite evident.

A graph of the output of a typical diode versus exposure time to a constant source is presented in Figure 14. The maximum residual from a least-square fit to the data points is only about 0.2 percent of the saturation signal for the system and occurs at the lowest signal level, where electronic noise becomes troublesome. Thus the intrinsic linearity of the array itself is probably better than 0.2 percent. Since there is every reason to believe that this linear performance will extend over the entire dynamic range of the photodiode, a system having as much as an order of magnitude greater dynamic range while retaining excellent linearity can clearly be realized if analog electronics of sufficient slew range and low noise can be designed.

Dark Leakage Current

While cooling the array to temperatures below 150°K should be sufficient to eliminate any significant amount of dark leakage current from the output signal, the possibility of anomolous leakage due to surface, edge, and space-charge layer effects still exists. A series of tests was therefore conducted with integration times of up to six hours to determine the extent of any residual dark leakage. These tests

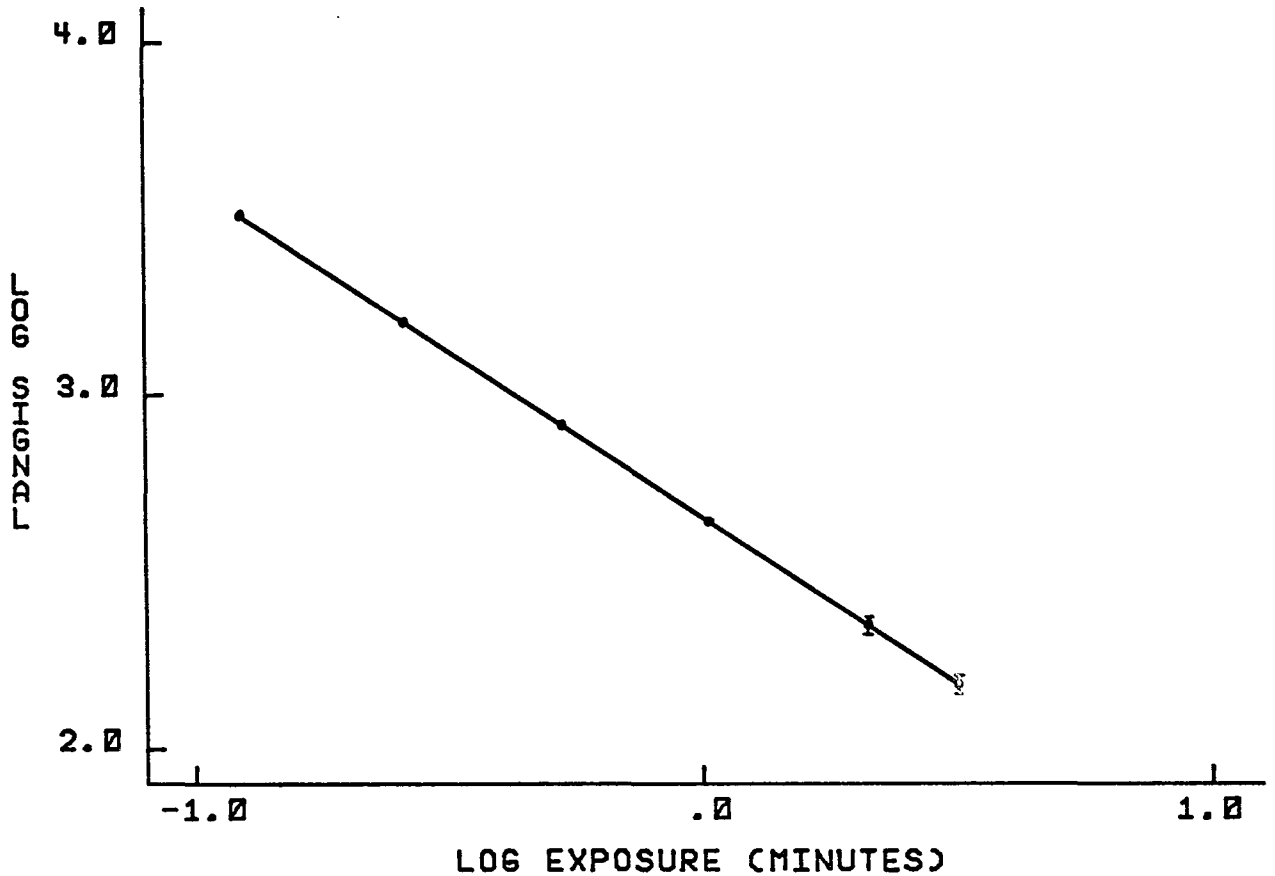

Fig. 14. Linearity Test: Log Signal (Counts) versus Log Exposure (Minutes) for a Typical Diode Element.

revealed that no measurable dark leakage current was present over integration times of several hours but that the DC shifts in the preamplifier mentioned above might prove troublesome. Provided the measures outlined above were taken to minimize the DC drift, it is evident that the goal of essentially zero dark leakage signal over reasonable integration times has been achieved.

Spatial Variations

Previous investigations indicated that the diode-to-diode variations in sensitivity are on the order of 1-2 percent over the entire length of typical photodiode arrays (Høg and Wiskott 1974; Dravins 1975). However, in these studies a fairly broadband source of illumination was used to conduct the tests. Since it was anticipated that interference effects from SiO_2 overcoating on the array would be present, a series of tests was conducted to determine the nature and extent of such variations in sensitivity as functions of wavelength. A Jarell-Ash monochromator having a bandpass of 16 Å was used to illuminate a diffusing screen in front of the RL-128L, producing a uniform field on the detector to a very good approximation. The results of two such scans are presented in Figure 15, one at 7100 Å and the second at 7600 Å. These scans show two basic features of the sensitivity variations which can be expected to be found in similar devices. That portion of the sensitivity variation that can be ascribed to the diodes themselves is indeed small, on the order of 2 percent RMS, as indicated by the scatter about a best-fit curve through the data points. Superimposed on this is an interference effect arising in the SiO_2 overcoating, resulting in

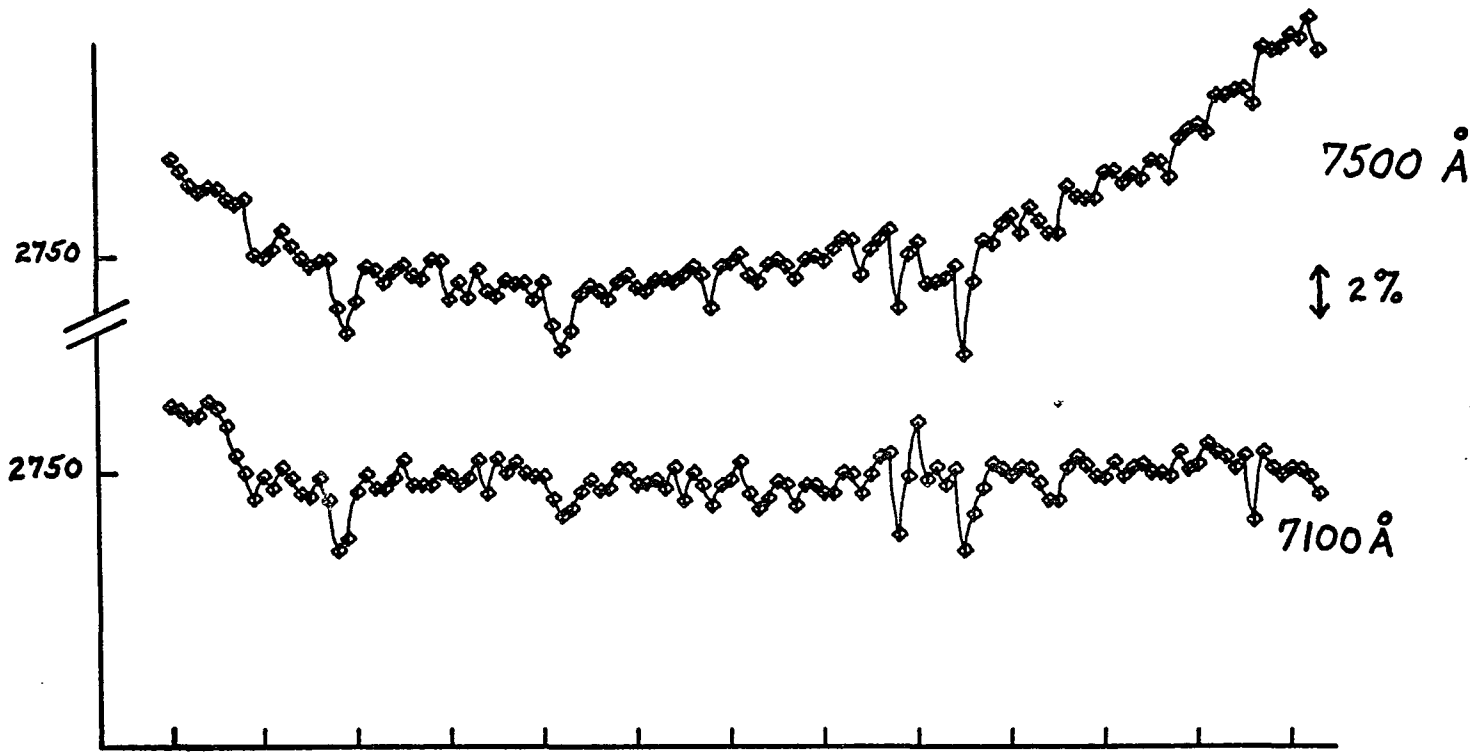

Fig. 15. Diode Sensitivity Variations at Different Wavelengths.

variations in sensitivity of individual diodes as a function of wavelength. These variations, however, are not all of the same magnitude across the array, resulting in a change in the shape of array response for a complete scan as a function of wavelength. This effect can clearly be seen in Figure 15. Although the entire array manifests an interference effect as a function of wavelength (as will be seen below), a differential pattern along the array is quite evident, especially at the edges where the sensitivity to interference seems to be greatest. It is therefore evident that the effects of these two types of interdiode variations in sensitivity, both the intrinsic diode sensitivity variations and chromatic variations from interference effects in the SiO_2 overcoating, must be considered in any calibration scheme for spectroscopic work or other observational configurations where the illumination is highly monochromatic. It is further evident that this calibration must be done using the optical configuration that will be used for making actual telescopic observations, since the magnitude of the interference effects in the overcoating will be sensitive to the nature of the beam (e.g. focal ratio) being focused on the diode array.

Absolute Quantum Efficiency

The determination of the absolute quantum efficiency of the RL-128L was a three-step process involving a relative sensitivity determination using the Jarrell-Ash monochromator with stabilized light source, a relative determination of the monochromator output function, and finally an absolute determination of the monochromatic flux incident on the array at a particular wavelength. The first step of this process

consisted of a series of long exposures, varying from 3 to 15 minutes in duration, using the attenuated beam of the monochromator to illuminate a small diffusing screen and scanning in wavelength by 100 Å steps. Exposure times were adjusted so that a large signal was obtained for each step in order to minimize the effects of electronic noise. The relative output of the monochromator was then determined using an IL 700 radiometer with a silicon detector head, calibrated against an NBS standard head at the University of Arizona Optical Science Center. The combination of the RL-128L response and the relative output of the Jarrell-Ash monochromator then yields the relative sensitivity of the array as a function of wavelength. To convert this to an absolute sensitivity requires only that the absolute flux at one wavelength be determined. This was done at 5500 Å using the IL 700 with phototube head because the level of illumination provided by the monochromator was insufficient to produce a large enough signal with the silicon head. The absolute flux at the plane of the RL-128L was thus determined to be 8.8×10^{-11} W/cm^2 sec which produced an average signal count of 1892 on the A/D converter, or 3.2×10^6 photons detected out of 5.1×10^6 photons/diode incident. Therefore, the absolute quantum efficiency of the cooled RL-128L is approximately 63 percent at 5500 Å, with the values at other wavelengths then determined by the relative sensitivity measurements. These results are displayed in Figure 16 for a typical diode in the array.

For the cooled RL-128L, peak quantum efficiency occurs near 7200 Å with a value of 83 ± 5 percent. The IR cutoff shows the effects of the cooling, with the measured quantum efficiency falling by a factor of

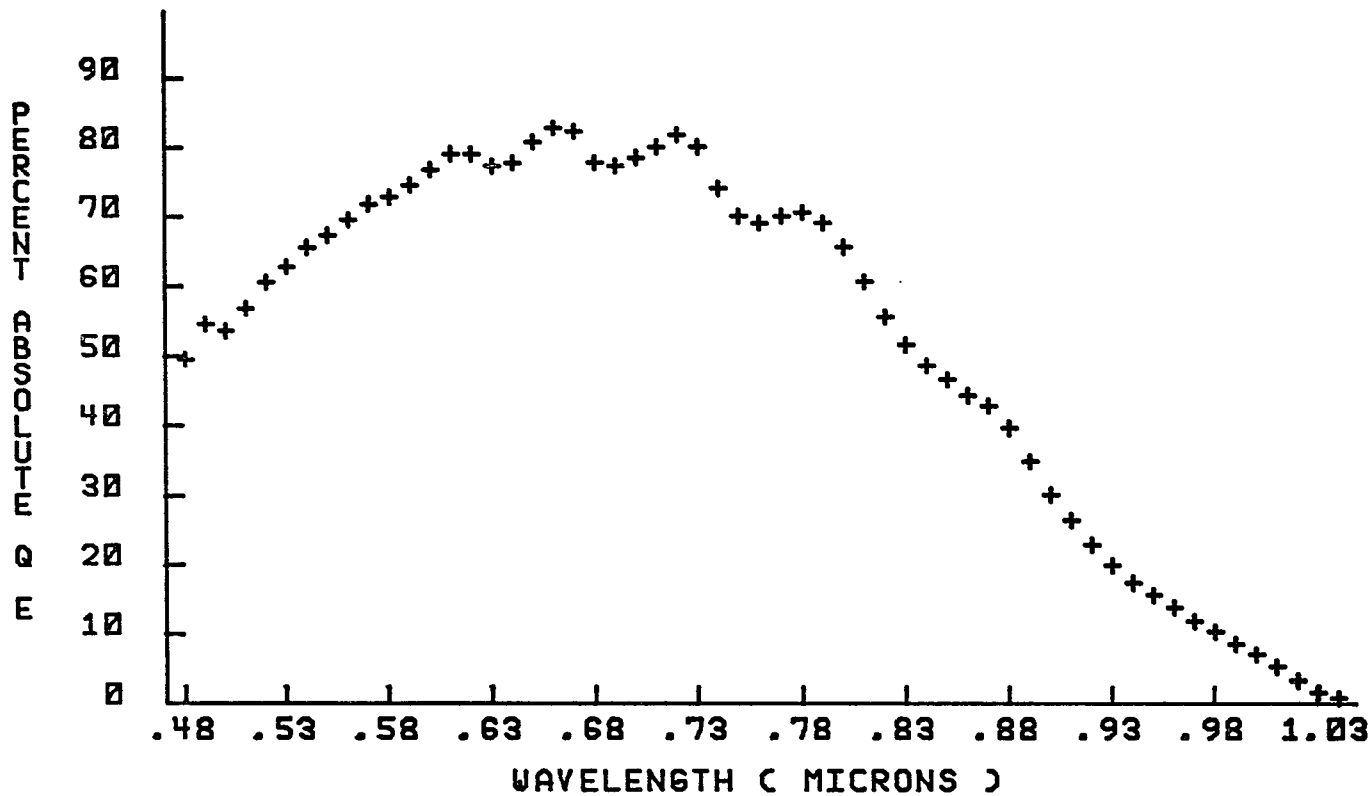

Fig. 16. Absolute Quantum Efficiency versus Wavelength for a Typical Diode Element.

ten from the peak value in the region of 10,000 Å. At approximately 0°C this same point is not reached until 10,800 Å (Livingston 1975) indicating that the behavior predicted by Equation 6 is confirmed approximately.

Because the illuminating screen used for this measurement subtended a solid angle of only about 6° square, the interference effects caused by the SiO_2 overcoating are quite pronounced, causing a peak-to-peak modulation of the sensitivity curve of approximately 6 percent. The peak quantum efficiency quoted above is measured at the maximum of one of these interference fringes. The periodicity of this modulation, although not the amplitude because of the uncollimated source, can be predicted by using the Stokes treatment of reflection from a thin film of SiO_2 (n = 1.45) deposited on a thick layer of Si (n = 3.9). The following relation then holds for transmission of collimated radiation of unit amplitude incident upon a layer of thickness d and index n_1 over the substrate material of index n_2:

$$I_T = 1 - \frac{r_1^2 + r_2^2 + 2r_1r_2 \cos \delta}{1 + r_1^2r_2^2 + 2r_1r_2 \cos \delta} \qquad (19)$$

where r_1^2 and r_2^2 are the reflectivities of the first and second boundaries, respectively, as given by Equation 2, and $\delta = [(4 \pi n_1 d)/\lambda] + \phi$. This relation is displayed in Figure 17 along with the observed interference features, extracted from Figure 16. Best fit to the period of the empirical interference pattern was obtained for a value of $d = 2.80\ \mu$, close to the nominal value of 3 μ for the SiO_2 overcoating,

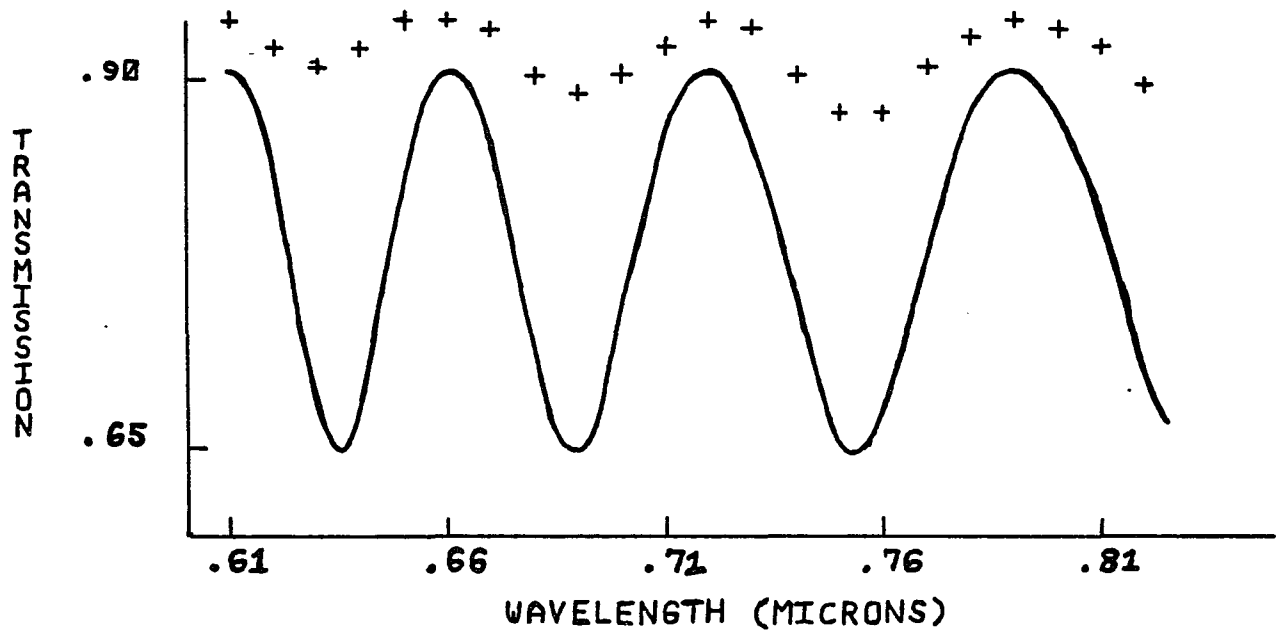

Fig. 17. Modulation of Transmitted Intensity: 2.80 μ SiO_2 Overcoating on Silicon.

provided by Snow (1975). Thus, the validity of the postulated interference mechanism is confirmed.

Spatial Response

Because the diode junctions of an integrated array share a common substrate in which much of the photogeneration of carriers takes place, the spatial resolution will vary with wavelength. Carriers generated deep in the substrate will in general have a greater chance of lateral diffusion to a neighboring diode than those generated nearer the diode junction. It is therefore expected that the spatial resolution should be degraded somewhat toward the IR cutoff as the absorption coefficient falls and photons penetrate deeper into the substrate.

The spatial response of the RL-128L was measured by scanning a narrow slit along the array and then graphing the resultant signals as a function of spatial phase. The projected slit width was made as narrow as possible (~ 6 μ) so that, to first order, the resultant spatial response curves represent the true deconvolved spatial response. The Jarrell-Ash monochromator was again used as the illuminating source in order to study the chromatic dependence. The spatial response curves thus generated reveal that the predicted loss in resolution toward the IR is indeed present. It was also noted that both the form and the chromatic behavior of the diode spatial response was essentially constant across the array. The findings for a typical diode are displayed graphically in Figures 18 through 22, covering the spectral interval of 6500 Å to 10,000 Å. These figures show the normalized diode response as a function of the spatial phase of the instantaneous slit position; 0.0

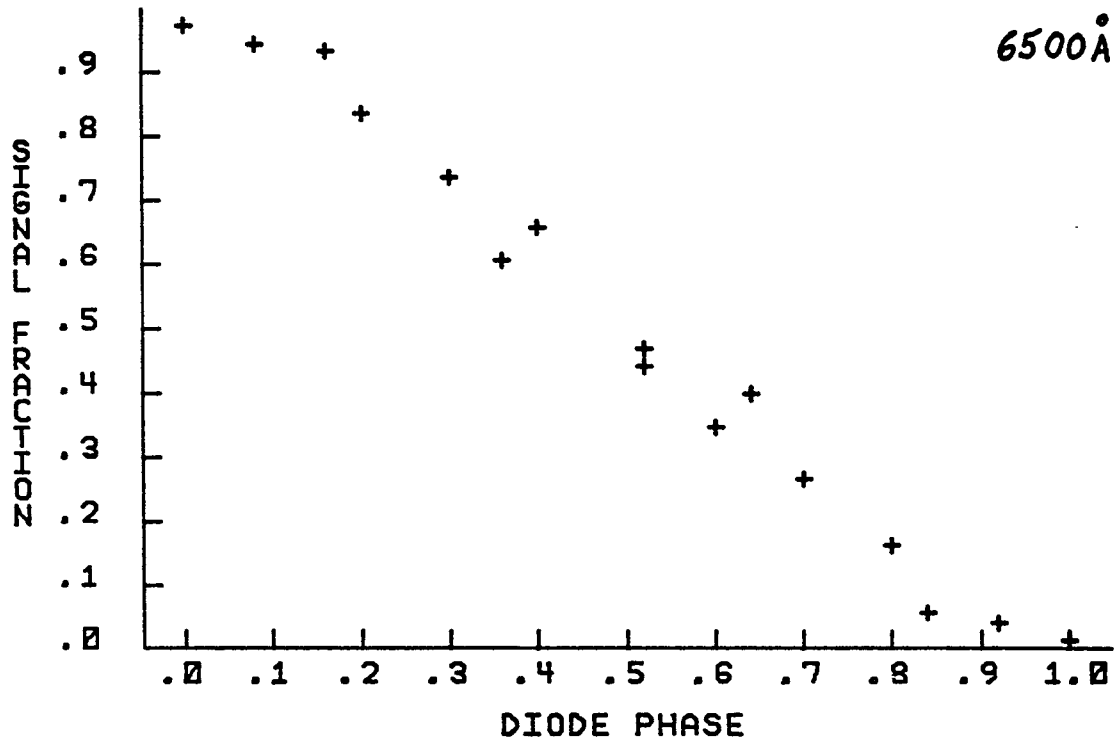

Fig. 18. Normalized Spatial Response (6500 Å).

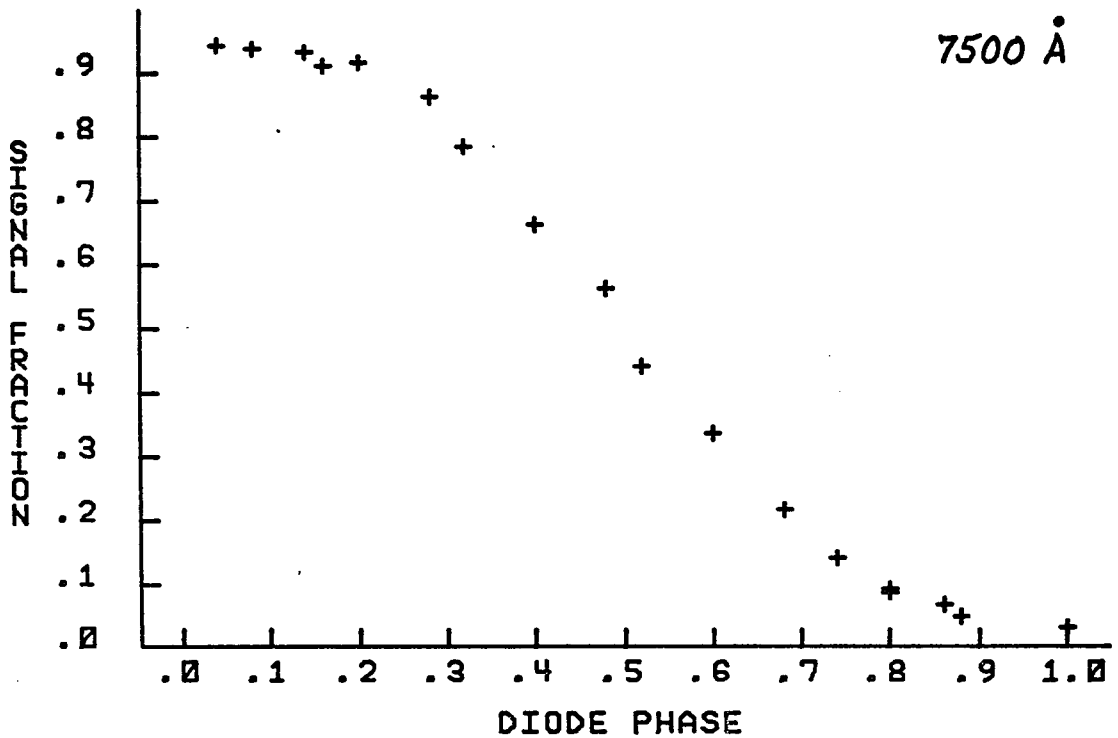

Fig. 19. Normalized Spatial Response (7500 Å).

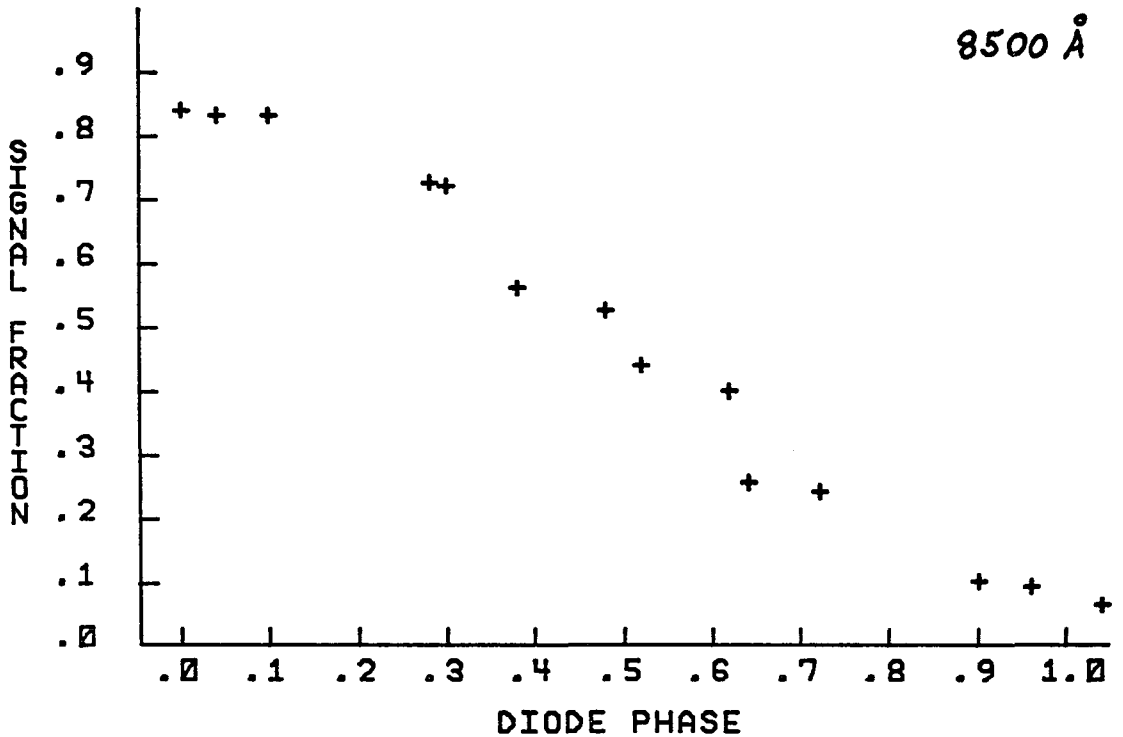

Fig. 20. Normalized Spatial Response (8500 Å).

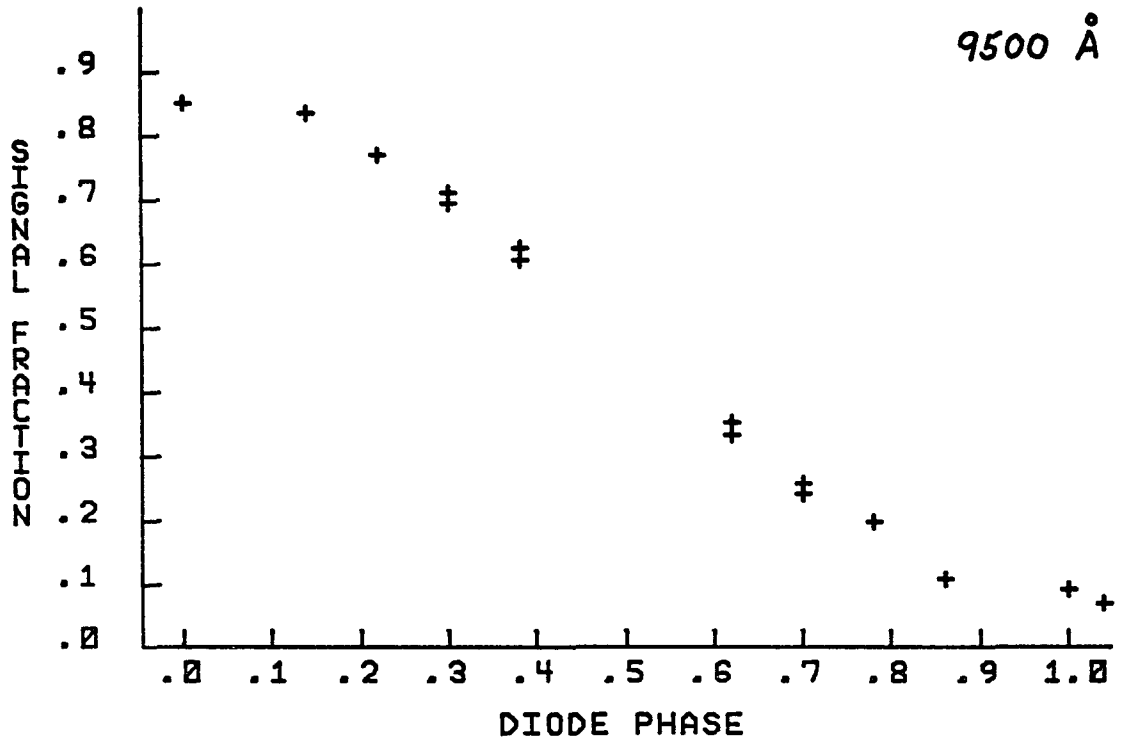

Fig. 21. Normalized Spatial Response (9500 Å).

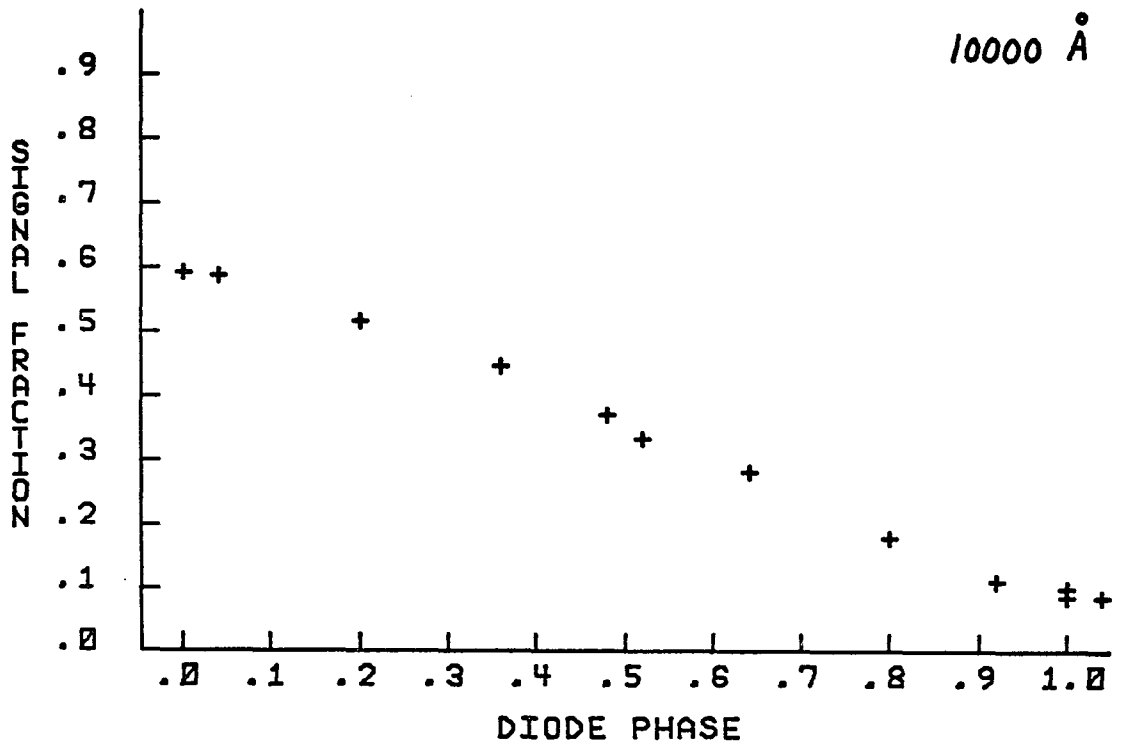

Fig. 22. Normalized Spatial Response (10,000 Å).

phase is arbitrarily taken to be the diode center, with phase 0.5 then representing the diode edges and 1.0 the centers of the adjacent diodes.

While a drop in spatial resolution seems to be present throughout the above spectral region as one moves toward the red, the effect is most pronounced just as the cutoff is reached, as can be seen in the rapid change between Figure 21 (9500 Å) and Figure 22 (10,000 Å). Over this short wavelength interval, the fraction of the signal collected from a slit placed on the diode center drops from 0.86 to 0.59, with the remainder of the generated charge diffusing laterally to adjacent diodes. A qualitative explanation for this behavior is not difficult to formulate, but a more complete treatment unfortunately requires determination of the diffusion parameters of the device, a task beyond the scope of this work. The characteristic slow decrease in spatial resolution toward the red with a rapid drop as the IR cutoff is approached is likely due to the relatively wide diode spacing in comparison to the diffusion length. This wide spacing makes it difficult for a carrier to diffuse laterally to the next diode unless it is generated quite deeply in the substrate, as would be the case at 10,000 Å, for instance. However, as can be seen from Figure 16, the quantum efficiency has fallen by an order of magnitude at this point, indicating that most of these photons penetrate to a depth greater than the diffusion length.

Since the values of bulk parameters like the diffusion length are likely to be fairly uniform for devices manufactured by the same techniques, one might therefore expect to find an even more pronounced drop in spatial resolution toward the red for devices having smaller

diode spacing than the RL-128L. The overall quantum efficiency curve will probably remain essentially unchanged but the region of rapidly falling spatial resolution will be shifted to shorter wavelengths. Livingston et al. (1975), using an array having 25 μ pitch, seem to confirm this view in that the MTF measured shows a rapid drop as far as 1500 Å away from the IR cutoff as compared to perhaps 500 Å to 1000 Å for the RL-128L (63.5 μ pitch). This effect therefore tends to place a lower limit on the diode pitch that can be effectively utilized in the IR near the cutoff, a fact that should be kept in mind when specifying an array to be used in this spectral region.

Detective Quantum Efficiency

Although the absolute quantum efficiency of a detector is of great importance in computing response characteristics, it is often difficult to compare the relative utility of various detectors using this quantity alone because it does not include information about system noise. For this reason, the concept of detective quantum efficiency (DQE) has been developed as a figure of merit for detector systems (Rose 1946; Jones 1959). In terms of the signal-to-noise ratios at the input and output of a detector system, the detective quantum efficiency is given by the equation:

$$DQE \equiv \frac{(S/N)^2_{out}}{(S/N)^2_{in}} \tag{20}$$

This quantity will numerically equal the absolute quantum efficiency

only in the case of a perfectly noiseless detector, a situation never realized in actuality.

The deviation of the DQE from the value of the absolute quantum efficiency at low light levels will be most severe for detectors such as the RL-128L system with a relatively high fixed electronic noise level compared to the photon shot noise of the input signal. For all signal levels except those very near the saturation level of the photodiodes themselves, the measured ENC of the RL-128L system is in fact larger than the corresponding photon shot noise, indicating that the true utility of this detector system will quite rapidly deteriorate at low illumination levels. The value of the DQE, in the case where night sky background may be neglected, can be computed from the following relation:

$$DQE = \frac{(\eta S_*)^2}{\eta S_* + (ENC)^2} \div (\eta S_*) = \frac{\eta S_*}{\eta S_* + (ENC)^2} \qquad (21)$$

Here, η is the absolute quantum efficiency and S_* is the total photon signal per diode element. A graph of the DQE versus S_* for $\eta = 0.80$ and (ENC) = 4760 is presented in Figure 23, showing the expected effects of system noise on DQE at low signal levels.

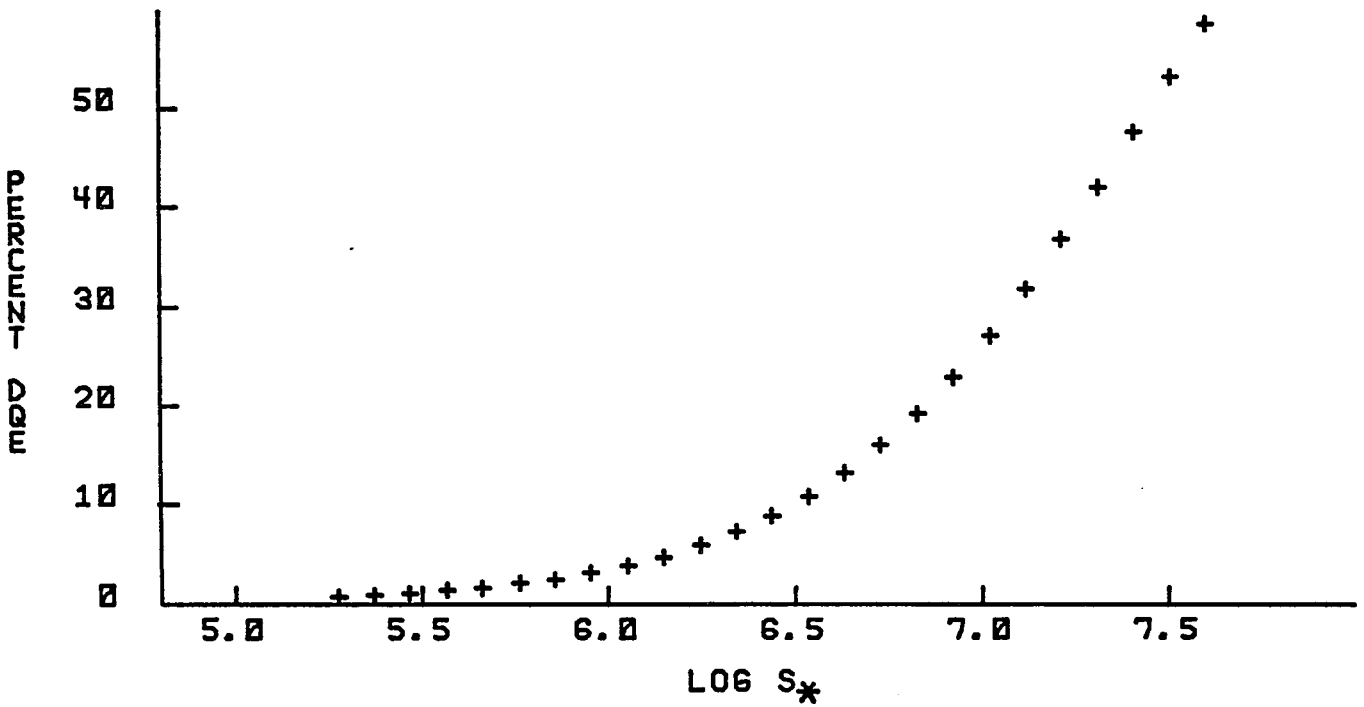

Fig 23. Detective Quantum Efficiency versus Log Total Photon Signal.

CHAPTER IV

OBSERVATIONAL EVALUATION

Spectrograph Configuration

The Cassegrain spectrograph for the 90-inch telescope at Steward Observatory is of conventional Boller and Chivens design, with a collimator of 3-inch diameter and 27 inch focal length to match the f/9 primary system for this telescope. The scale at the slit focus is approximately 10 arcsec/mm. The camera available for normal operation with this spectrograph proved to be unsuitable for use with the present RL-128L system. The problem here lies with the dewar container, in that it has proved impractical to mount the array closer to the entrance window than about 21 mm. Since the free focal distance for the Cassegrain-Schmidt camera available for this spectrograph is only 7 mm, the use of a substitute camera is required.

The camera constructed to remedy this problem consists of a Kodak Aero-Ektar f/2.5 lens of 12-inch focal length, mounted in a special purpose housing which also furnishes the mechanical interface to the dewar container. This particular lens was chosen because it is inexpensive, readily available, and well suited to the problem at hand. With the entrance aperture stopped to approximately 100 mm to match the typical exit pupil of the gratings used, the intrinsic resolution of the camera is approximately 55 μ in the red spectral region. This resolution is certainly adequate for the RL-128L, with 63.5 μ diode pitch, and

in fact results in undersampling to some extent unless the entrance slit is opened to match the projected diode spacing.

The major problems introduced by a refractive camera are chromatic effects, especially changes in the focal length of the camera as a function of wavelength. In the red and near IR, the gradient of the axial shift in focal length with wavelength is found to be approximately +0.5 mm/1000 Å. This range of chromatic focus shift can fortunately be handled by the collimator focus adjustment alone for the entire spectral region of primary interest, approximately 6000 Å to the IR cutoff at about 10,200 Å, where photographic plates and photoemissive surfaces have great difficulty in working effectively. However, care must still be taken in establishing the best possible focus across the photodiode array, even one as short as the RL-128L. In practice, it proved possible to establish a diode-limited focus for the entire array with a spectral bandpass as large as 630 Å. Correct focus was established by monitoring the width of the comparison lines and adjusting the collimator focus for the narrowest profiles across the array. This procedure proved to be necessary for every 100 Å shift in central wavelength, but the resultant settings proved reproducible thereafter provided gratings were not interchanged. In practice it proved possible to resolve sharp spectral features quite readily, as will be evident later (see Figs. 24, 26, 27, and 28).

Because of the square aspect ratio of this particular photodiode array, alignment of a stellar spectrum along the array was anticipated to be a problem, and an opposing setscrew adjustment for array tilt was

therefore built into the mechanical interface between dewar and camera. The method for determining the residual tilt between the spectrum of a continuum lamp and the diode array involves comparing the output with the array fully illuminated to the output with the array partially obscured by a sliding stop in the plane of the entrance slit. A misalignment will result in a noticeable relative tilt being evident in the graphical displays of the two spectra while a proper alignment will result in only an attenuation in signal but no change in the relative shape of the observed spectral distribution between the unobscured and partially obscured spectra. After the proper alignment is obtained by means of the setscrew adjustment, the moveable stop is positioned so that the continuum source again illuminates the array fully but without extending further in order to provide a spatial reference along the slit for stellar objects. Placing a star at the junction of the stop and the entrance slit then insures that the array is fully illuminated.

Two diffraction gratings are available for the spectrograph which proved to be suitable for use with this system, one having 832 lines/mm and producing a reciprocal dispersion of 2.48 Å/diode, the other having 400 lines/mm and producing a reciprocal dispersion of 4.90 Å/diode, both gratings being operated in the first order. Because of the broad spectral sensitivity of the detector, one or more filters must be inserted into the system in order to block the second order blue spectrum when working in the first order red region.

With a focal length of 308 mm, the Aero-Ektar camera produces a slit demagnification factor of 2.25 for this spectrograph. The

projected diode elements therefore cover an area 143 μ square at the slit, or 1.43 arcsec square. The actual slit setting used for observations conformed to this value to the accuracy of the micrometer adjustment, there being little point in making the spectrographic resolution elements much smaller than the detector resolution. The resultant throughput at the slit was therefore quite good during periods of average or better seeing, when the seeing disk is typically less than 2 arcsec in diameter.

Atmospheric Absorption and Emission

Work in the near IR spectral region requires some attention be paid to the effects of atmospheric absorption and emission. In the region between 6000 Å and 10,200 Å, the three principle absorption features are the A- and B-bands of O_2 and the strong water vapor band between 9000 Å and 9600 Å. The B-band at 6868 Å presents no great observational problem, but the A-band at 7595 Å extends over a range of 100 Å and may absorb as much as 70 percent of the incident radiation, making most observations in this region impossible. The water vapor band, however, is an even more serious problem, both because it is broad and strong (50 percent or more attenuation) and because it is of highly variable strength in both time and sky position. It is therefore best to avoid this region, if possible, because even differential spectral measurements are very difficult.

In addition to these absorption features, many night-sky emission lines and bands, chiefly due to OH, become strong in the near IR (Broadfoot and Kendall 1968). The continuum upon which these features

are impressed is also increasing toward the red, rising by a factor of more than 100 between 4000 Å and 10,000 Å, reaching a level of approximately 40 R/Å at the latter wavelength. This emission corresponds in brightness to approximately m = 17/arcsec^2 in the near IR continuum and perhaps 1 magnitude brighter in the stronger OH lines. Thus, with a projected resolution area of 2.0 arcsec^2, the contribution of night-sky emission will only start to become significant for objects fainter than 12th magnitude or so, and then only in spectral regions where there are strong lines or a high continuum level such as is found at wavelengths longward of 9000 Å.

Calibration

The ideal way to determine the relative sensitivity characteristics of the RL-128L array elements is to observe a standard steller source of known flux and spectrum. A number of such sources, mostly white dwarf starts or faint O-type starts showing essentially continuous spectra, have been extensively observed in order to provide spectrophotometric calibration standards (Oke 1974; Stone 1974). Unfortunately, none of these sources proved bright enough in the red and near IR to give an acceptable S/N ratio in reasonable integration times with the RL-128L. Several very bright standards having extensive spectrophotometric data available were also observed, but the presence of many absorption features in the spectra makes their use difficult for a sensitivity calibration of individual diode elements, especially since the absolute calibration of these sources has in every case been done with much lower resolution than in this system.

Because of the above difficulties, an alternative calibration method involving the use of a continuum lamp illuminating the slit of the spectrograph was adopted. Such a method is capable of providing a true relative calibration of the individual diode sensitivity referenced to the spectrograph slit if the true relative spectrum of the illuminating source is known. Such a calibrated source which can be properly fitted to the spectrograph unfortunately is not presently available. A source of constant, but unknown, spectrum and intensity was therefore used to produce a differential diode response function, although one not referenced to the spectrograph slit but instead containing instrumental effects such as the grating efficiency and the chromatic camera profile. Over short wavelength intervals, however, such as found within a spectrum taken at a fixed grating angle, this sort of calibration is sufficient to at least furnish accurate differential information about spectral features.

The calibration problem thus resolves itself into finding the differential response of each diode element of the array relative to the average response of all other diodes to the same wavelength interval. This relative response is then weighted by the average quantum efficiency across the array at the wavelength of interest (interpolated from the measured absolute quantum efficiency at 100 Å intervals), to produce a final diode-by-diode table of correction factors to be used at a given grating tilt setting on the spectrograph. While the application of this table of correction factors to an observation will not produce a resultant spectrum which relates in a simple way to a true spectral intensity

at the slit of the spectrograph, a differential flux determination between observed spectral features and nearby continuum should be quite good.

The actual procedure used to generate the tables of differential correction factors involved the measurement of the spectrum of the constant source at small steps in grating tilt, bracketing the grating tilt of interest so that a complete sweep of all relevant wavelengths across the array was accomplished. The grating tilt was increased by 0.02° per step, corresponding to a wavelength shift of 15 Å for the 400 line/mm grating used. The resultant information was written in sequential blocks on magnetic tape and a FORTH program written which then searched through the data blocks, reading out the response of each diode to every wavelength interval within the passband of the central grating setting. The preliminary correction factors generated were then applied to the original signals at the grating setting of interest and a 5-point running average low-pass filter applied to partially remove the effects of variable grating efficiency on the data, thereby producing a smooth curve representing the spectrum of the continuum source. An inspection of the distribution of points about a curve fitted through the final smoothed spectrum revealed that the RMS deviation was less than 0.2 percent of full scale after a single filtering step. The resultant final correction factors were stored on magnetic tape to be utilized as needed for observations using the same grating tilt.

Observational Tests

As an initial program at the spectrograph, the spectra of the argon, neon, and xenon comparison sources were mapped from 6000 Å to 10,000 Å. This not only served to determine the wavelength intervals covered by the array at various grating tilts but also allowed a table of collimator focus settings versus wavelength to be generated for future observations. The mechanical construction of the detector system and camera proved to be stable enough that these focus settings and grating tilts were repeatable, even after removing and remounting the camera.

The actual observational program to test the performance of the complete system consisted of observations of progressively fainter sources to see at what point system noise became troublesome. For integration times on the order of 30 minutes, this point proved to be around $m_v = 10$, where a signal-to-noise ratio of 50 or so could be obtained under good seeing conditions. An observation was also made of an emission line object, NGC 7009, the Saturn Nebula. This planetary nebula has a surface brightness of approximately $16^m/\text{arcsec}^2$, among the brightest available. Several spectra were obtained along the minor axis of this nebula in order to determine the response of the array to such a source, one of which is presented in Figure 24. The most prominent features are the [Ar III] λ7135 and HeI λ7065 lines, but HeI λ7283 and the [OII] doublet λλ7319, 7330 are clearly detected. The ratio of intensities for the strong [Ar III] and HeI features is approximately 0.30, in excellent agreement with the scanner observations near the same area of the nebula recently made by Aller and Epps (1975). I have not

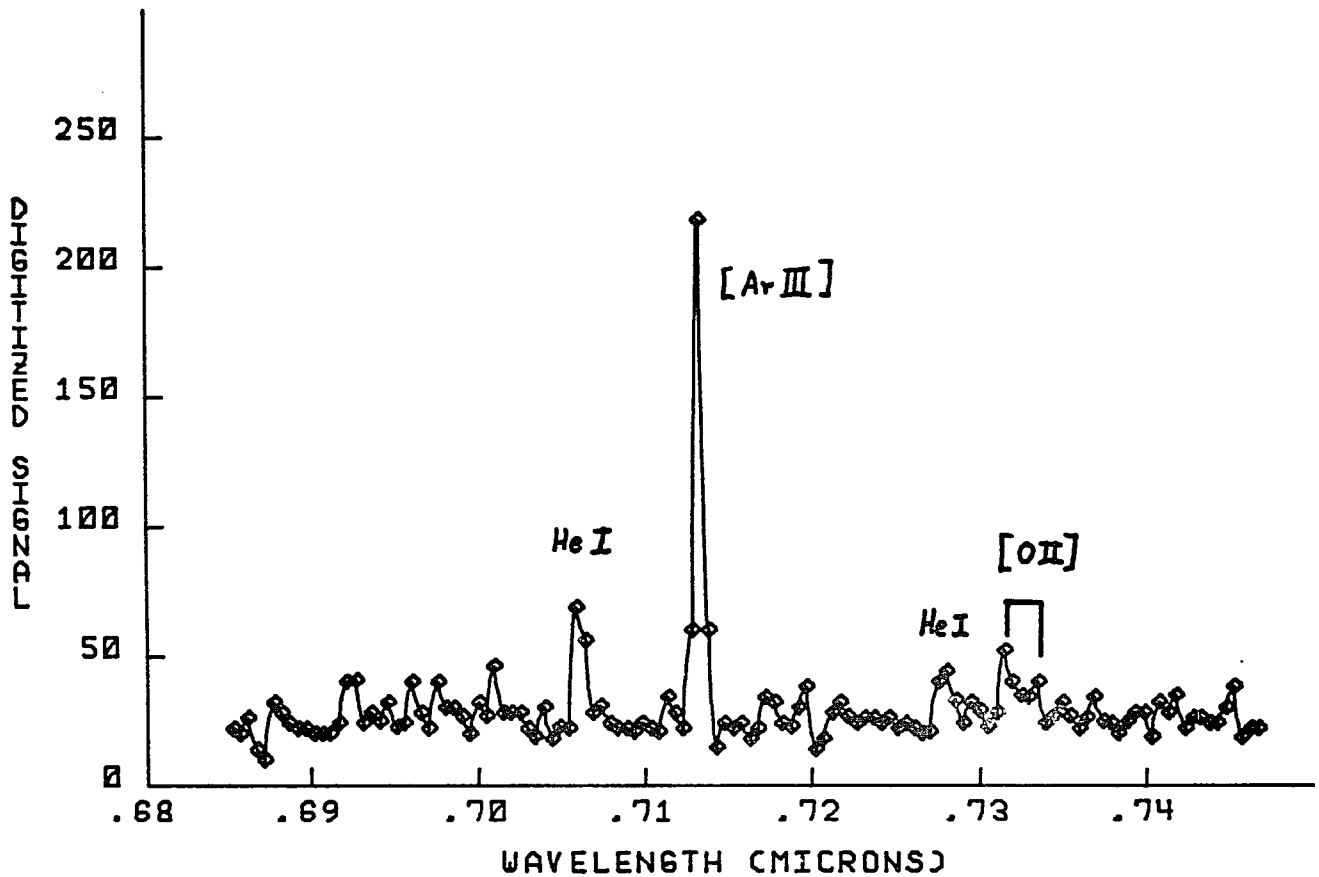

Fig. 24. NGC 7009 (Saturn Nebula), 30 Minute Exposure.

succeeded in finding any plausible identifications for the features shortward λ7065 and the reality of any of these lines is therefore questionable. Much longer integration times than the 30 minute exposure used here would be necessary to clarify the nature of the continuum in this region.

At the request of another institution, a number of M-type giant variables were observed, both to get some idea of the shape of the spectra in the near IR and to serve as a starting point for determining secular changes. At the same time, I decided to test the feasibility of computer-controlled rapid scanning and so a program was devised to automatically scan the array periodically and write the data onto tape, with a concurrent display registered on a monitor screen in order to check for saturation conditions. The minimum integration time utilizing this program was about 2 seconds, set by the cycle time of the tape drive, so that only objects having red magnitudes greater than 2.5 or so could be observed. Once the proper exposure time was established, the computer could then control the entire data acquisition sequence, with the total number of scans so generated limited only by the availability of magnetic tape and the patience of the observer.

In playing back some of this recorded information on a display monitor, it was evident that an unwanted tilt had been introduced into the spectra, probably due to a slight misalignment of the array with respect to the stellar spectrum. However, when several sequential scans were averaged, the composite spectra seemed to show few residual tilt effects, thereby making possible some comparisons of spectra taken at

different times but without the high time resolution originally planned. One star with particularly extensive data, EU Del, an M6 III SR variable of 59.5 day period, was checked for spectral variability, both within the short time covered by the observations at one grating setting (approximately 30 minutes) and between the two successive nights on which such rapid scans were made. No convincing evidence for spectral variations within the short time span of one night's observations could be found, but quite definite changes were noted in the spectra taken on successive nights, at least in one spectral region. Figure 25 shows a composite average of 20 scans of EU Del on each of the two nights, covering the spectral region λλ6817-7437. The average values of the ordinates across the array were arbitrarily forced to agree and no further adjustments of the baselines have been made prior to graphing the data. While instrumental or atmospheric absorption effects cannot be ruled out as the cause of the apparent change in this particular band, neither can the validity of this variation be totally discounted, especially in view of the close agreement between similar spectra taken at longer wavelengths. Figure 26 illustrates this close agreement between averaged scans from the two night's observations over the wavelength range λλ8036-8660. The same procedure of force fitting the average values was utilized here with quite different results. Because of the close agreement between these two composite spectra, symbols have been omitted in Figure 25 to avoid confusion.

As a final project during the operational testing of the RL-128L system, some blue objects were selected for observation both to check

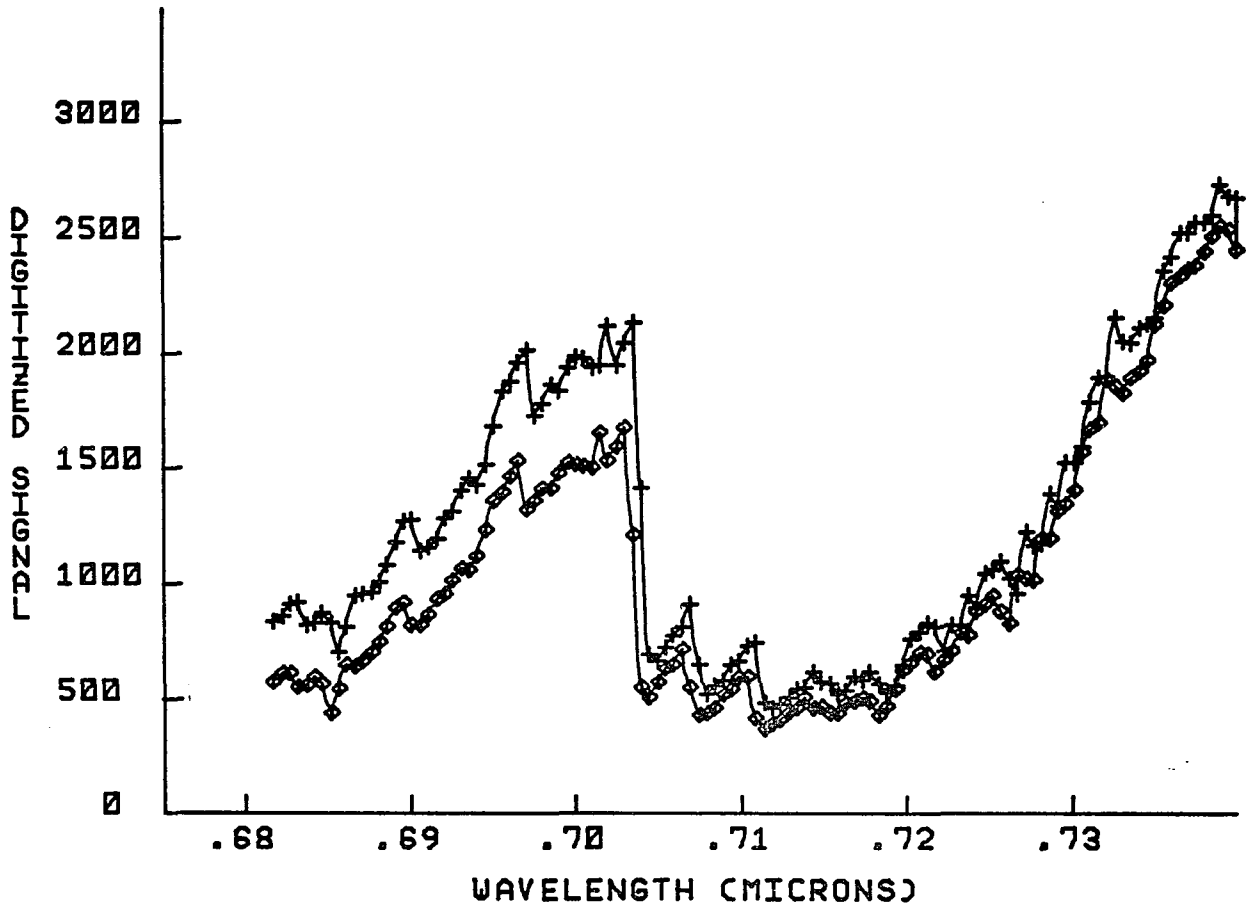

Fig. 25. Composite Spectra of EU Del, Successive Nights (λλ6817-7437).

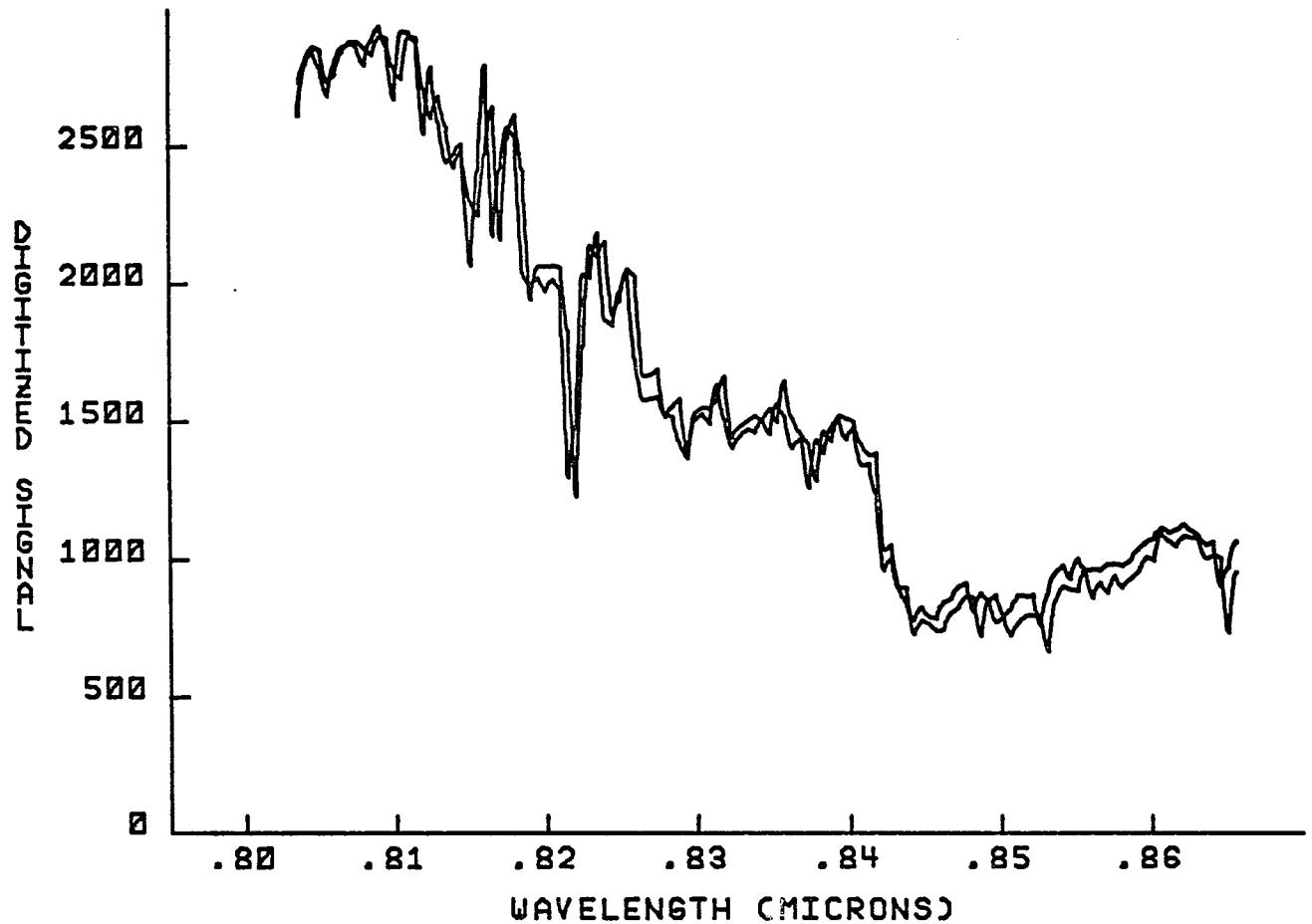

Fig. 26. Composite Spectra of EU Del, Successive Nights (λλ8036-8660).

the exposure times required for obtaining good IR spectra and to possibly look for some interstellar features in the near IR, a topic not extensively studied in the past. For this latter problem, a pair of stars was selected, one highly reddened and one essentially unreddened. HD 183143, a B7 Ia star of $m_v = 6.9$ having $E_{B-V} = +1.36$, has been extensively studied recently in the visible by Herbig (1966, 1975) and York (1971) and exhibits a wide variety of strong interstellar features. The comparison star chosen, HD 164353, is an unreddened B5 Ib object of $m_v = 3.9$ and $E_{B-V} = +0.10$. Spectra of these two starts at λλ6817-7437 and λλ8036-8660 are presented in Figures 27 and 28. The displayed spectra for HD 164353 are averages of five separate scans, while those for HD 183143 are single observations of 5 minutes duration.

In Figure 27, the feature at λ7120 ± 2 in HD 183143 can possibly be ascribed to interstellar absorption. The only likely atomic transition which could be found is a line of CI at λ7118.5. However, this particular transition does not arise from the ground state, indicating that the observed line is either stellar in origin or is a diffuse interstellar feature. The latter interpretation is favored because of the absence of other CI lines in the visible spectrum of HD 183143.

A second possible interstellar feature can be seen in the spectrum of HD 183143 in Figure 28 near λ8620. No reasonable atomic line occurs at or near this wavelength, a fact that tends to rule out an atomic transition as the source of this feature, either stellar or interstellar. It is therefore strongly indicated that this feature is also due to molecular or solid-state transitions which produce the other diffuse features seen previously at shorter wavelengths.

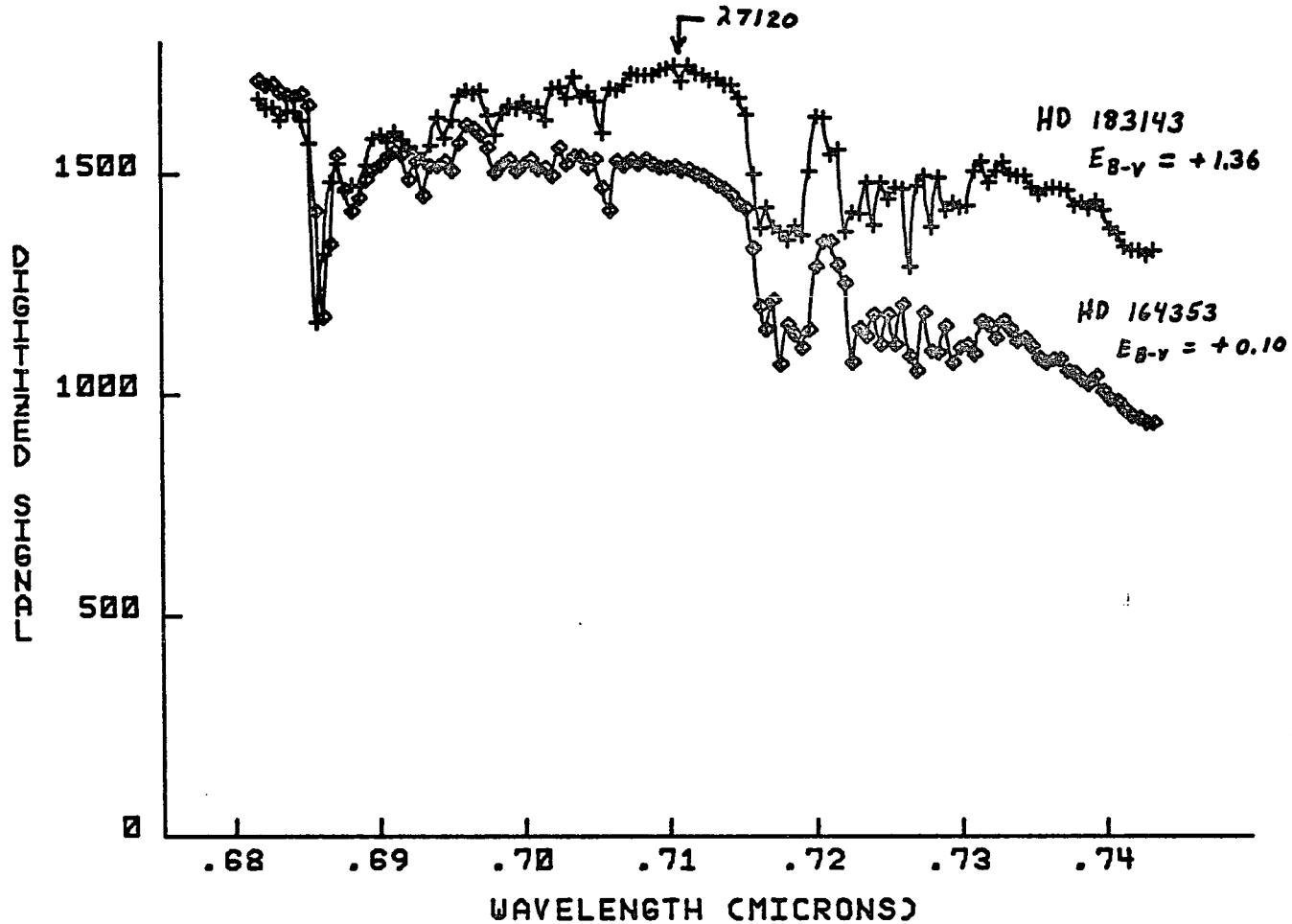

Fig. 27. Spectra of Reddened and Unreddened B-Type Supergiants (λλ6817-7437).

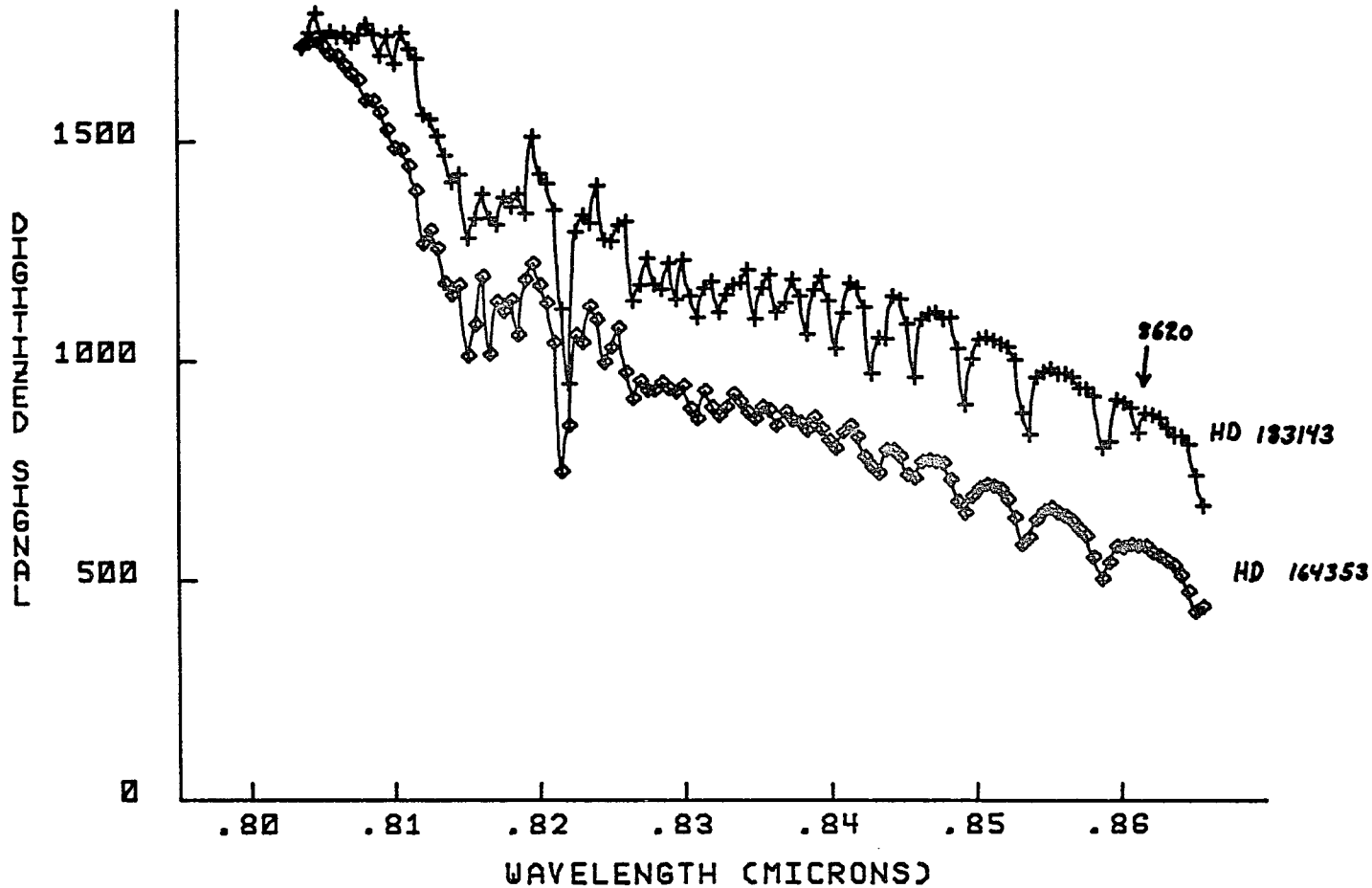

Fig. 28. Spectra of Reddened and Unreddened B-Type Supergiants (λλ8036-8660).

CHAPTER V

CONCLUSIONS

The results of the laboratory and spectrographic tests on the RL-128L system indicate that the expectations of high quantum efficiency, essentially linear response over a large dynamic range, and simplicity of data processing can be realized in an operational system suitable for use at the telescope. The peak quantum efficiency has been determined to be approximately 83 percent at 7200 Å, making the photodiode array the most efficient detector available in the visible and near IR regions of the spectrum. The inherent linearity of the detector coupled with the high quantum efficiency and broad dynamic range make such a system particularly useful in studying phenomena of small amplitude and requiring accuracy comparable to that found previously only with photoelectric spectrum scanners, especially in the near IR where photoemissive surfaces become inefficient. While this type device cannot be used for work on very faint sources due to the relatively high level of noise introduced as a consequence of the readout procedure, it remains a tool of considerable utility for work on brighter sources where the large signal available results in a high DQE.

The presence of an interference effect in the spectral response of the RL-128L requires the use of a careful calibration technique to remove it from spectrographic records. Such effects can probably be expected from all devices of similar manufacture. This interference

arises from the reflection of incident light from the front silicon surface and the SiO_2 overcoating which is a few microns thick. The resultant modulation of diode sensitivity proved to be repeatable only for a fixed optical configuration, thus requiring that the calibration of relative diode response as a function of wavelength be accomplished using the observational optical system.

While the extreme degree of cooling used in this investigation was successful in effectively eliminating dark leakage current from the output video, even for long integrations, an unfortunate loss in IR sensitivity resulted. It should be recognized that cooling to such low temperatures will not be required for work on objects of medium brightness where integration times of only a few minutes at most are required for a strong signal. The desirability of a cooling method which would allow a range of temperatures down to the region of liquid nitrogen is clearly indicated in order to allow the dark leakage current and IR sensitivity cutoff to be adjusted to fit the observing program.

As mentioned in the preceeding discussion of the steller observations, the square aspect ratio of the diode elements of this particular array posed an alignment problem that was not entirely resolved during the investigation. Since an alignment tied to the illumination provided by a continuum source proved to be somewhat inaccurate, the only alternative for this particular device appears to be an alignment on an actual steller spectrum. Due to the inevitable effects of camera flexure, this sort of procedure must then be repeated for every major movement of the telescope. However, this problem should essentially

disappear if an array having long, narrow diodes is utilized instead, a design feature that can readily be incorporated into any future system.

While the overall system noise was reduced to a level sufficiently small that observations of good quality could be made on stars as faint as 10th magnitude and emission-line sources down to 16th magnitude over exposure times on the order of 30 minutes, further improvements should be attempted in order to extend the useful range of such devices to fainter sources. However, it is evident that at best only an order of magnitude improvement can be expected due to the high shunt capacitance of such devices and the lack of a low noise preamplifier integrated on the array itself. A gain in system flexibility is also possible in the area of increased dynamic range through the use of signal processing electronics of sufficient slew range to more fully match the inherent range of the photodiodes. The present electronic configuration utilized only about 10 percent of the full range of the photodiodes and yet possessed a dynamic range in excess of 1000. It is evident that a small decrease in system noise coupled with increased electronic range can then yield a system with a dynamic range of several times 10^4 for a single integration.

Probably the most pleasant discovery during the course of this investigation was the ease with which spectrographic records could be accumulated and the information compiled and reduced using the computer. On one night alone over 700 individual spectra were obtained and it is not impossible that this number might rise into the thousands in the future, especially for a program requiring high time resolution on fairly

bright sources. Because of the fixed format and stable sensitivity, reducing and displaying a very large amount of such data is a relatively simple matter. Finally, the completely linear response of the detector allows such operations as averaging, adding, and differencing of spectra to be accomplished in an easy and straightforward manner with the computer.

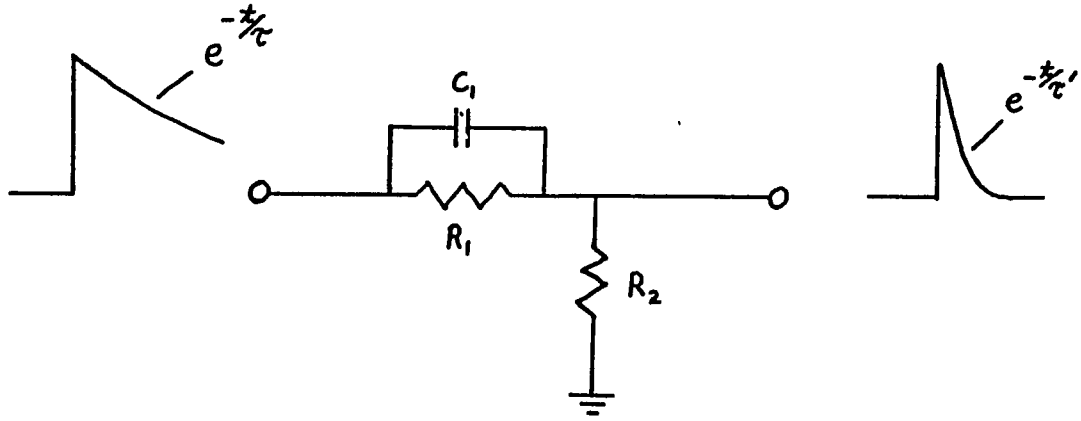

If $R_1C_1 = \tau$, then $\tau' = k\tau$, where $k = \dfrac{R_2}{R_1 + R_2}$.

APPENDIX A. Pole-Zero Cancellation Network.

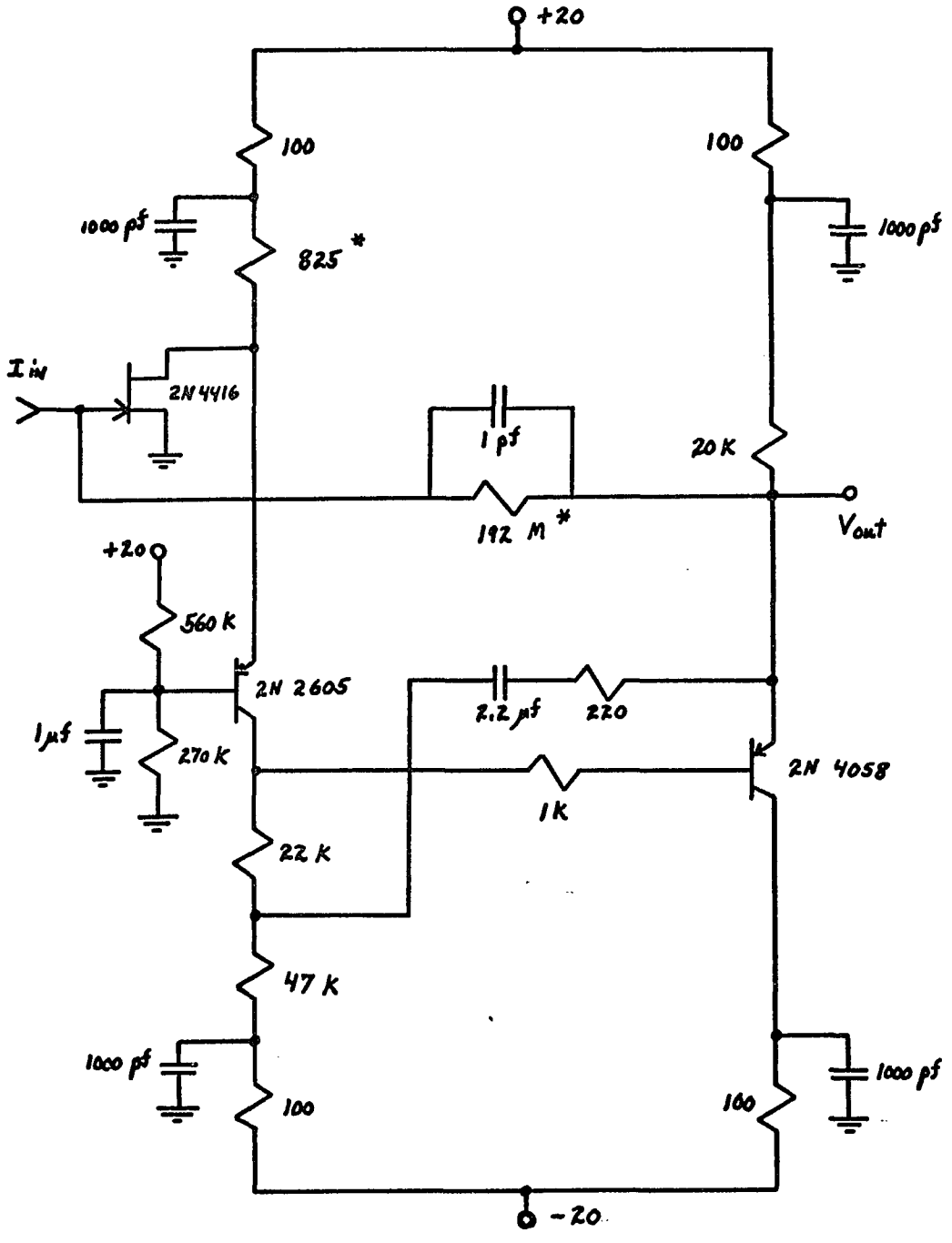

APPENDIX B. Preamplifier Schematic.

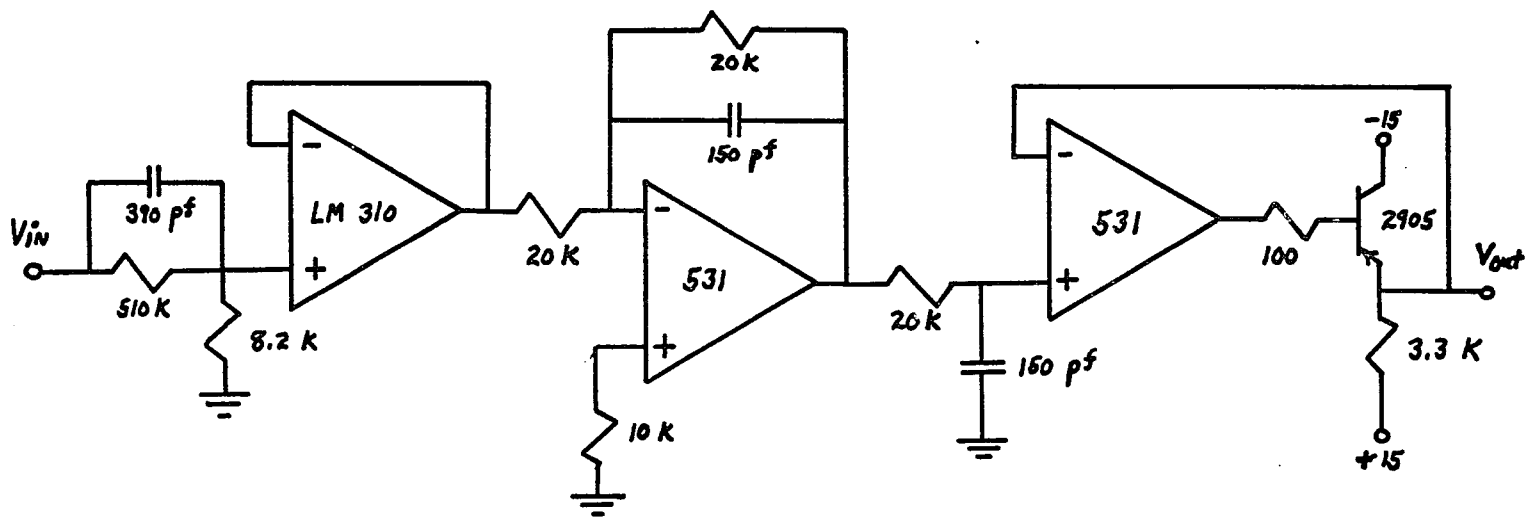

APPENDIX C. Filter Network.

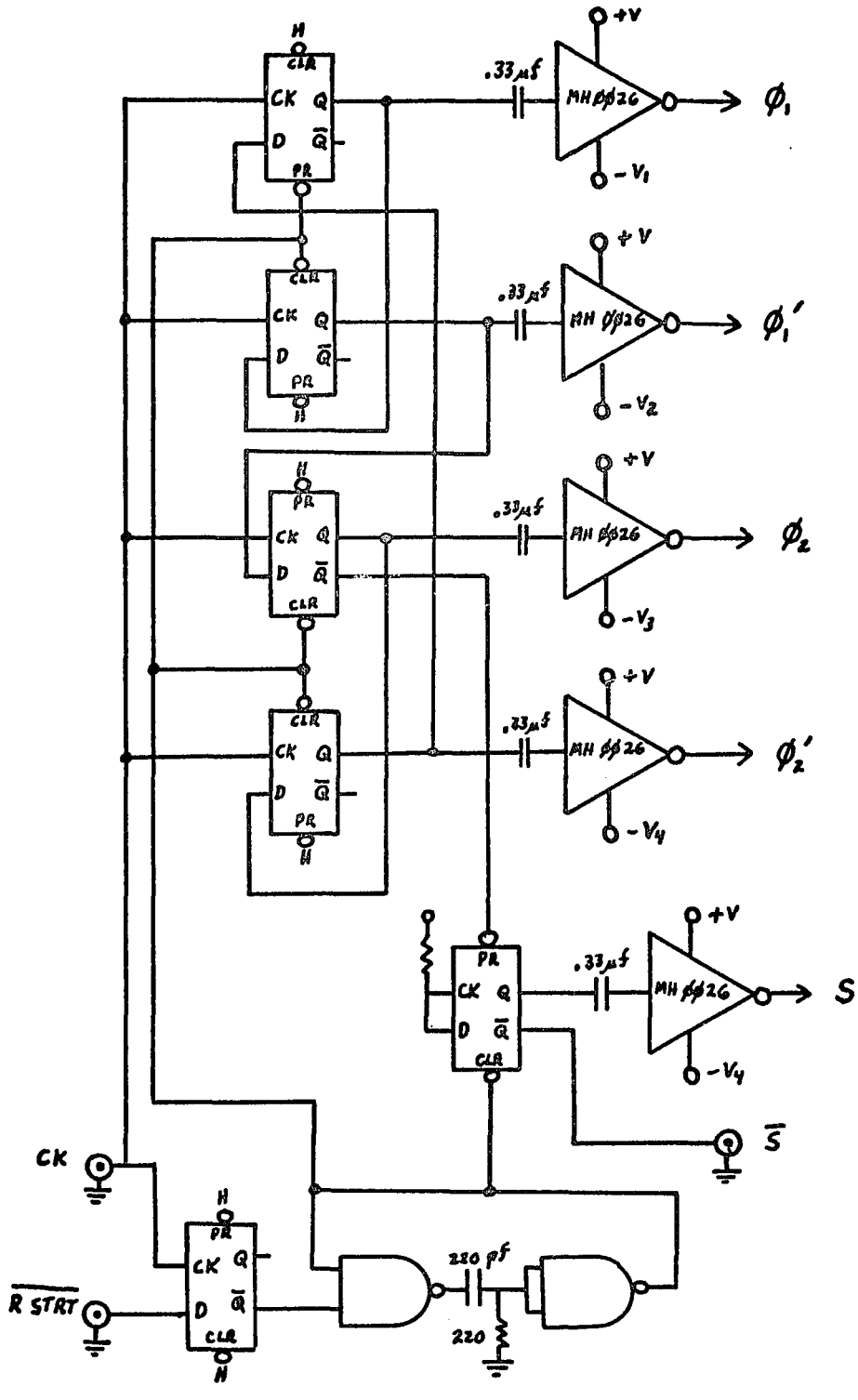

APPENDIX D. Drive Circuitry.

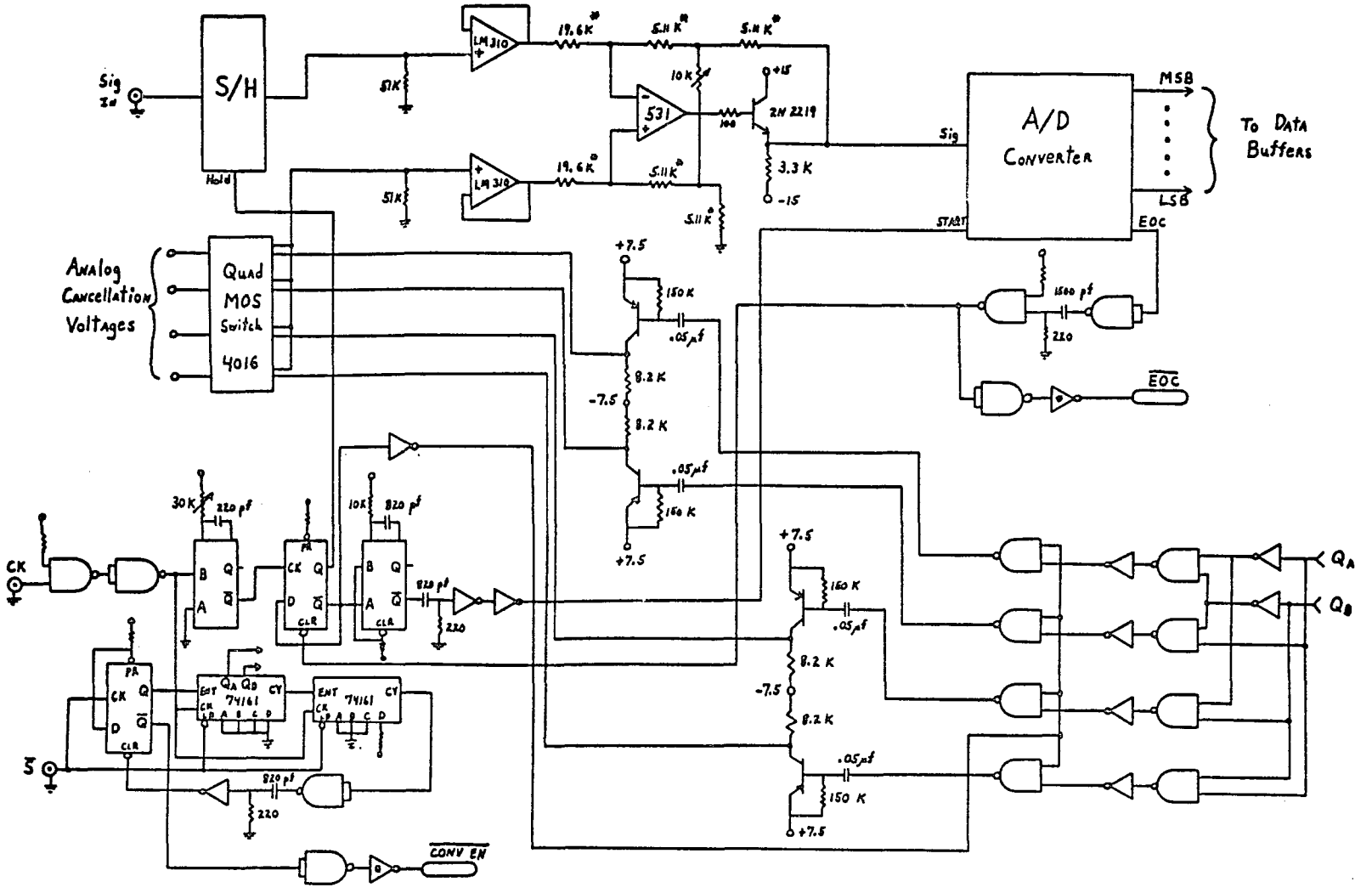

APPENDIX E. A/D Conversion Module.

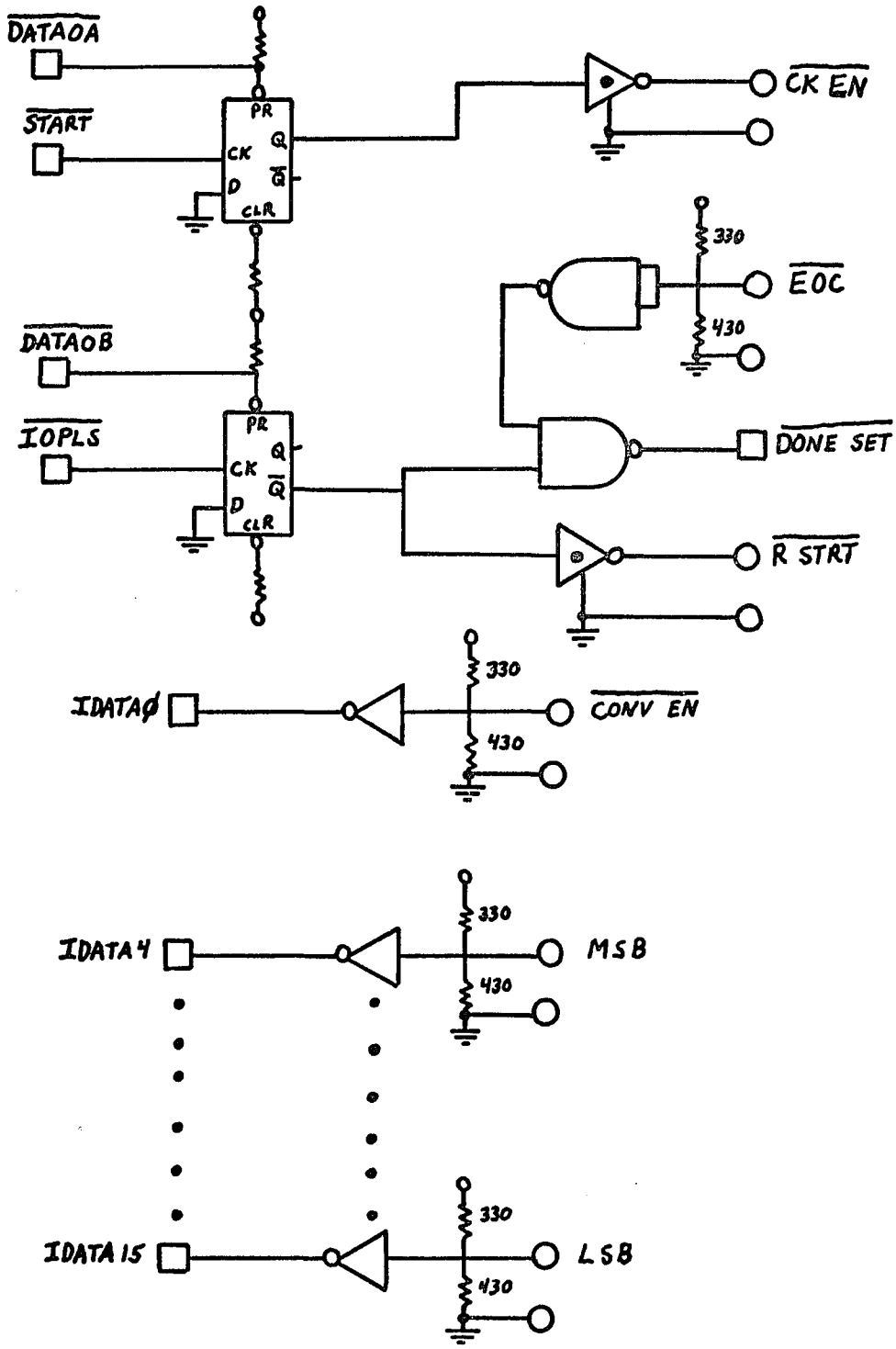

APPENDIX F. Computer Interface.

REFERENCES

Aitkin, D. W. 1968, IEEE Trans. Nucl. Sci., NS-15(3), 10.

Aller, L. H., and Epps, H. W. 1975, Ap. J., 197, 175.

Ambroziak, A. 1968, Semiconductor Photoelectric Devices (London: Iliffe).

Beaver, E. A. 1973, Astronomical Observations with Television-type Sensors, ed. J. W. Glaspey and G. A. H. Walker (Institute of Astronomy and Space Science, U. of British Columbia), p. 55.

Boksenberg, A. 1970, Astronomical Use of Television-type Image Sensors, ed. V. R. Boscarino (Princeton University), NASA SP-256, p. 77.

Broadfoot, A. L., and Kendall, K. R. 1968, J. Geophys. Res., 73, 426.

Bube, R. H. 1960, Photoconductivity of Solids (New York: Wiley).

Callahan, D. E., and Torley, J. R. 1968, IEEE Trans. Electron Devices, ED-15, 248.

Cole, T. W., and Ables, J. G. 1974, Astr. and Ap., 34, 149.

Cromwell, R. H. 1969, Ph.D. dissertation, U. of Arizona.

Cromwell, R. H., and Dyvig, R. R. 1973, U. of Arizona Optical Sciences Center, Technical Report 81.

Dash, W. C., and Newman, R. 1955, Phys. Rev., 99, 1151.

Dravins, D. 1975, Conference on "Image Processing Techniques in Astronomy," Utrecht (24-27 March 1975).

Dyck, R. H., and Weckler, G. P. 1968, IEEE Trans. Electron Devices, ED-15, 196.

Fan, H. Y., Shepherd, M. L., and Spitzer, W. 1956, Photoconductivity Conference, (New York: Wiley).

Gilbert, G. R. 1973, Astronomical Observations with Television-type Sensors, ed. J. W. Glaspey and G. A. H. Walker (Institute of Astronomy and Space Science, U. of British Columbia), p. 83.

Gilbert, G. R. 1975, Bull. A.A.S., 7, No. 3, Part 1, p. 442 (Abstract).

Goulding, F. S. 1966, Nucl. Instr. and Methods, 43, 1.

Goulding, F. S., Walton, J. T., and Pehl, R. H. 1970, IEEE Trans. Nucl. Sci., NS-17(1), 218.

Herbig, G. H. 1966, Zs. f. Ap., 64, 512.

Herbig, G. H. 1975, Ap. J., 196, 129.

Høg, E., and Wiskott, D. 1974, Eur. S. Obs. Tech. Rep. No. 5.

Hunten, D. M. 1972, unpublished memorandum, Kitt Peak National Observatory.

Jones, R. C. 1958, Phot. Sci. and Eng., 2, 57 (No. 2).

Jones, R. C. 1959, Adv. El. and El. Phys., 11, 87.

Kern, H. E., and McKenzie, J. M. 1974, IEEE Trans. Nucl. Sci., NS-21, 260.

Kleinknecht, H., and Seiler, K. 1954, Z. Physik, 139, 599.

Livingston, W. C. 1975, Kitt Peak National Observatory (private conversation).

Livingston, W. C., Harvey, J., Slaughter, C., and Trumbo, D. 1975, Appl. Optics (in press).

Lowrance, J. L. 1973, Astronomical Observations with Television-type Sensors, ed. J. W. Glaspey and G. A. H. Walker (Institute of Astronomy and Space Science, U. of British Columbia), p. 5.

McCord, T. R., and Bosel, J. 1973, Astronomical Observations with Television-type Sensors, ed. J. W. Glaspey and G. A. H. Walker (Institute of Astronomy and Space Science, U. of British Columbia), p. 137.

McNall, J. F. 1973, Astronomical Observations with Television-type Sensors, ed. J. W. Glaspey and G. A. H. Walker (Institute of Astronomy and Space Science, U. of British Columbia), p. 115.

Mende, S. B., and Shelley, E. G. 1975, Appl. Optics, 14, 691.

Moss, T. S. 1959, Optical Properties of Semiconductors (London: Butterworth Scientific Publications Ltd.).

Noble, P. J. W. 1968, IEEE Trans. Electron Devices, ED-15, 202.

Oke, J. B. 1974, Ap. J. Suppl. #36, 27, 21.

Pell, E. M. 1956, J. Appl. Phys., 27, 768.

Robinson, L., and Wampler, E. J. 1972, Pub. A.S.P., 84, 497.

Rose, A. 1946, J. Soc. Motion Picture Engrs., 47, 273.

Smithson, R. C. 1975, Solar Phys., 40, 241.

Snow, E. H. 1975, Vice President for Operations, Reticon Corporation (private conversation).

Stone, R. P. S. 1974, Ap. J., 193, 135.

Title, A. M. 1974, Solar Phys., 35, 233.

Tull, R. D. 1975, U. of Texas, (private conversation).

Tull, R. D., and Nather, R. E. 1973, Astronomical Observations with Television-type Sensors, ed. J. W. Glaspey and G. A. H. Walker (Institute of Astronomy and Space Science, U. of British Columbia), p. 171.

van der Ziel, A. 1962, Proc. IRE, 50, 1808.

Weckler, G. P. 1967, IEEE J. Solid-State Circuits, SC-2, 65.

Weimer, P. K., Sadasiv, G., Meyer, J. E., Meray-Horvath, L., and Pike, W. S. 1967, Proc. IEEE, 55, 1591.

York, D. G. 1971, Ap. J., 166, 65.

Zweig, H. J., Higgins, G. C., and MacAdam, D. L. 1958, J. Opt. Soc. Am., 48, 926.